



Swansea University  
Prifysgol Abertawe



## Cronfa - Swansea University Open Access Repository

---

This is an author produced version of a paper published in:

*Small*

Cronfa URL for this paper:

<http://cronfa.swan.ac.uk/Record/cronfa48048>

---

### Paper:

Traini, G., Ruiz-de-Angulo, A., Blanco-Canosa, J., Zamacola Bascarán, K., Molinaro, A., Silipo, A., Escors, D. & Mareque-Rivas, J. (2018). Cancer Immunotherapy of TLR4 Agonist-Antigen Constructs Enhanced with Pathogen-Mimicking Magnetite Nanoparticles and Checkpoint Blockade of PD-L1. *Small*, 1803993

<http://dx.doi.org/10.1002/sml.201803993>

Released under the terms of a Creative Commons AttributionNonCommercial License (CC-BY-NC).

---

This item is brought to you by Swansea University. Any person downloading material is agreeing to abide by the terms of the repository licence. Copies of full text items may be used or reproduced in any format or medium, without prior permission for personal research or study, educational or non-commercial purposes only. The copyright for any work remains with the original author unless otherwise specified. The full-text must not be sold in any format or medium without the formal permission of the copyright holder.

Permission for multiple reproductions should be obtained from the original author.

Authors are personally responsible for adhering to copyright and publisher restrictions when uploading content to the repository.

<http://www.swansea.ac.uk/library/researchsupport/ris-support/>

# Cancer Immunotherapy of TLR4 Agonist–Antigen Constructs Enhanced with Pathogen-Mimicking Magnetite Nanoparticles and Checkpoint Blockade of PD-L1

Giordano Traini, Ane Ruiz-de-Angulo, Juan Bautista Blanco-Canosa, Kepa Zamacola Bascarán, Antonio Molinaro, Alba Silipo, David Escors, and Juan C. Mareque-Rivas\*

Despite the tremendous potential of Toll-like receptor 4 (TLR4) agonists in vaccines, their efficacy as monotherapy to treat cancer has been limited. Only some lipopolysaccharides (LPS) isolated from particular bacterial strains or structures like monophosphoryl lipid A (MPLA) derived from lipooligosaccharide (LOS), avoid toxic overactivation of innate immune responses while retaining adequate immunogenicity to act as adjuvants. Here, different LOS structures are incorporated into nanoparticle-filled phospholipid micelles for efficient vaccine delivery and more potent cancer immunotherapy. The structurally unique LOS of the plant pathogen *Xcc* is incorporated into phospholipid micelles encapsulating iron oxide nanoparticles, producing stable pathogen-mimicking nanostructures suitable for targeting antigen presenting cells in the lymph nodes. The antigen is conjugated via a hydrazone bond, enabling rapid, easy-to-monitor and high-yield antigen ligation at low concentrations. The protective effect of these constructs is investigated against a highly aggressive model for tumor immunotherapy. The results show that the nanovaccines lead to a higher-level antigen-specific cytotoxic T lymphocyte (CTL) effector and memory responses, which when combined with abrogation of the immunosuppressive programmed death-ligand 1 (PD-L1), provide 100% long-term protection against repeated tumor challenge. This nanovaccine platform in combination with checkpoint inhibition of PD-L1 represents a promising approach to improve the cancer immunotherapy of TLR4 agonists.


excitement in immunotherapy, this therapy does not show significant clinical benefit in most patients when considering all cancer types as a whole (70–80%).<sup>[2]</sup> Moreover, the systemic delivery of the immunotherapy and the doses required to induce the host immune reactions against cancer can cause immune-related adverse effects.<sup>[3]</sup> Evidence is also emerging that some patients (~9%) become “hyper-progressors” after this immunotherapy. These patients show extremely poor clinical outcome and accelerated tumor growth after single-agent checkpoint inhibitor treatment.<sup>[4,5]</sup> In addition, late relapses are now emerging as the result of longer follow-up of clinical trial populations, which suggests the emergence of acquired resistance to these treatments.<sup>[6]</sup> A key opportunity is turning nonimmunogenic (cold) tumors into immunogenic (hot) tumors. However, the few adjuvants (immune potentiators or immunomodulators) that are used for human vaccines in licensed products have important drawbacks for application in cancer immunotherapy. They fail to stimulate or are

weak inducers of the cellular Th1 immune responses and CD8<sup>+</sup> T-cell responses required to mediate antitumor immunity.<sup>[7]</sup> Consequently, there is urgent need for new approaches to enhance the efficacy of vaccine adjuvants for activating immune responses against cancer and for combination immunotherapy approaches.

## 1. Introduction

Cancer immunotherapy, which attempts to harness the specificity and power of the immune system against cancer, is revolutionizing cancer treatment.<sup>[1]</sup> Although immune checkpoint blockade represents a breakthrough and accounts for much of the current

G. Traini, Dr. A. Ruiz-de-Angulo, Dr. J. B. Blanco-Canosa, K. Zamacola Bascarán  
CIC biomaGUNE  
Paseo Miramón 182, 20014 San Sebastián, Spain

 The ORCID identification number(s) for the author(s) of this article can be found under <https://doi.org/10.1002/sml.201803993>.

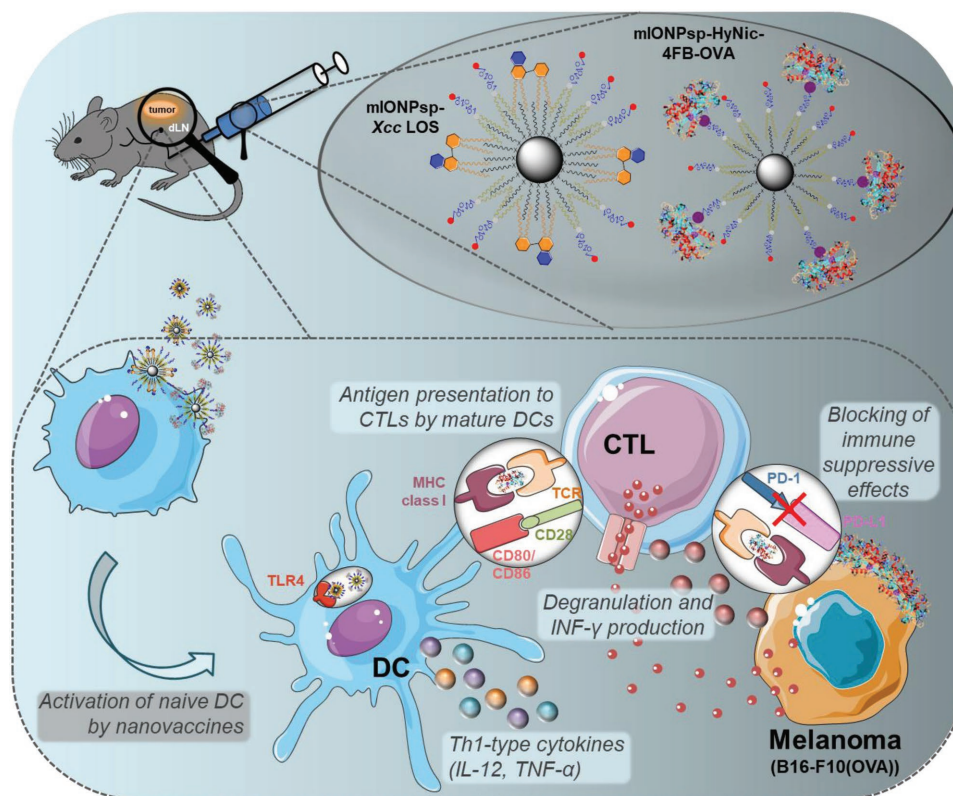
© 2018 The Authors. Published by WILEY-VCH Verlag GmbH & Co. KGaA, Weinheim. This is an open access article under the terms of the Creative Commons Attribution-NonCommercial License, which permits use, distribution and reproduction in any medium, provided the original work is properly cited and is not used for commercial purposes.

DOI: 10.1002/sml.201803993

A. Molinaro, A. Silipo  
Dipartimento di Scienze Chimiche  
Università di Napoli Federico II  
Complesso Universitario Monte Sant' Angelo  
Via Cintia 4, 80126 Napoli, Italy

Dr. D. Escors  
Navarrabiomed-Biomedical Research Centre  
Fundación Miguel Servet-IdISNA  
Complejo Hospitalario de Navarra  
31008 Pamplona, Spain

Prof. J. C. Mareque-Rivas  
Department of Chemistry and Centre for NanoHealth  
Swansea University  
Singleton Park, Swansea SA2 8PP, UK  
E-mail: [juan.mareque-rivas@swansea.ac.uk](mailto:juan.mareque-rivas@swansea.ac.uk)



**Scheme 1.** The pathogen-mimicking magnetite nanoparticles are designed to activate dendritic cells via TLR4 promoting trafficking to the draining lymph nodes. When administered with antigen-loaded nanoparticles prepared by a chemoselective ligation strategy, and in combination with the abrogation of tumor cell PD-L1 expression, they promote potent antitumor protective immunity. This figure was created using Servier Medical Art templates (<https://smart.servier.com>), which are licensed under a Creative Commons Attribution 3.0 Unported License: <https://creativecommons.org/licenses/by/3.0/>.

Toll-like receptor (TLR) agonists have been studied intensively as potential adjuvants for anticancer vaccines due to the known crucial roles of TLRs in both innate and adaptive immunity.<sup>[8,9]</sup> TLR agonists generate immune stimulatory effects through the induction of costimulatory molecules (CD80, CD86, and CD40) on dendritic cells (DCs) and inflammatory cytokines (TNF- $\alpha$  and IL-12) that favor the development of Th1 immune responses.<sup>[10]</sup> However, TLR agonists as monotherapies have so far seen limited success when tested in clinical trials, something that has been attributed to dose-limiting toxicities owing to systemic cytokine induction<sup>[11]</sup> and inefficient delivery to tumor and draining lymph nodes.<sup>[12]</sup> Moreover, new studies have shown that they can also induce immune inhibitory factors.<sup>[13]</sup> Improved delivery and blocking these immune suppressive effects of TLR agonists provide new opportunities to augment the anti-tumor effects of TLR agonists. On the other hand, several studies have found that cancer vaccines can significantly enhance the effects of checkpoint blockade,<sup>[14]</sup> and therefore combination of targeted cancer vaccines with immune checkpoint inhibitors promises to improve the efficacy and clinical benefit of immunotherapies. Although various nanoparticles (NPs) have been used as delivery vehicles of TLR agonists, the biocompatibility, complexity of synthesis and the efficacy when evaluated in animal models varies greatly.<sup>[15–22]</sup>

Another difficulty to achieve effective antitumor responses are cancer cells expressing suboptimal tumor antigen levels.<sup>[23]</sup>

This problem may be overcome if the NP also delivers tumor antigen to the LN-resident DCs so that they can activate and properly present antigen to T-cells to trigger a high-avidity anti-tumor response.<sup>[16,19,20,22,24–26]</sup>

To address these issues, here we adopt, optimize, and evaluate a micellar-based platform for improved codelivery of a TLR4 agonist and OVA as model antigen to the tumor and draining lymph nodes together with a strategy to evaluate the effect of interfering with the immune checkpoint programmed death-ligand 1 (PD-L1) (Scheme 1). Several formulations exploiting NPs (quantum dots (QDs), and superparamagnetic iron oxide nanospheres and nanocubes) encapsulation in polyethylene glycol-phospholipid (PEG-phospholipid) micelles were screened for the capture of the TLR4 agonists. The best nanovaccine was formulated using 6 nm magnetite NPs, a particle size, and a biocompatible and biodegradable material already used clinically in contrast agents for diagnosis by magnetic resonance imaging (MRI),<sup>[27,28]</sup> as iron supplement<sup>[29]</sup> and in hyperthermia treatments.<sup>[30,31]</sup> Moreover, some studies suggest that the intrinsic redox and magnetic properties of iron oxide NPs (IONPs) can be applied both to potentiate different cancer immunotherapies approaches, including DC-based vaccination<sup>[32]</sup> and macrophage polarization into pro-inflammatory M1 phenotypes.<sup>[33]</sup>

Many studies exploiting NP-mediated antigen delivery used amide bond formation between carboxylic acids and amines using

carbodiimide activation (e.g., 1-ethyl-3-(3 dimethylaminopropyl)-carbodiimide, or EDC); an approach that, to work properly, requires high and significant excess of reagents, and suffers from poor chemoselectivity and a high degree of cross-linking.<sup>[34]</sup> Additionally, the lack of suitable analytical methods to rapidly characterize the NP-antigen conjugates means that these reactions can be difficult to optimize, as they have to be performed without direct feedback on the progress of the reaction. To overcome these limitations, here we applied a bis-aryl hydrazone linkage strategy for the coupling of mIONPsp to the model antigen OVA with aniline as a nucleophilic catalyst.<sup>[35]</sup> The hydrazone linkage strategy provided important advantages for the formation of the antigen-nanoparticle conjugates. The reaction could be conveniently monitored by UV-vis with fast reaction kinetics and high yields (>85% in just a few minutes) of conjugation at neutral pH and micromolar concentrations, yielding stable conjugates.<sup>[34,35]</sup>

For development of cancer vaccines, many studies have investigated the use of lipopolysaccharides (LPS), which as major components of the cell surface of Gram-negative bacteria, exert immune stimulatory effects via engagement of TLR4. LPS (Figure 1a) is composed of three domains, an amphipathic domain known as lipid A, the hydrophilic O-antigen polysaccharide and a core oligosaccharide (OS) chain, connecting lipid A and O-antigen. Lipid A is responsible for the endotoxic activity of LPS and derivatives of this domain with reduced toxicity have been targets for the development of human vaccine adjuvants. Monophosphoryl lipid A (MPLA, Figure 1a), a detoxified derivative of Salmonella Minnesota LPS approved by the FDA for use in humans, has been evaluated as a cancer vaccine adjuvant in a number of clinical trials.<sup>[36]</sup> The best results were obtained with MPLA combined with alum, which led to boosted antibody responses.<sup>[37–39]</sup> However, effective anticancer vaccination requires also generation of robust T-cell immunity, and these systems have not consistently mediated potent antitumor immunity.<sup>[36,40]</sup> Lipooligosaccharides (LOS, Figure 1a), LPS not possessing the O-antigen chain (named rough LPS), have been investigated less for oncological indications.<sup>[41]</sup> Since the immune stimulatory effects and toxicity of LPS and LOS greatly vary and are linked to structural variations and physical states at the supramolecular structure level (i.e., its “state of aggregation”), here we explore the potential of *Escherichia coli* LOS and the plant pathogen *Xanthomonas campestris* pv. *campestris* (Xcc) LOS as anticancer vaccine adjuvants. We reasoned that differences in these LPS structures could not only affect the biological activity but also regulate the incorporation into the NP-filled phospholipid micelle delivery vehicles (mNPs). Moreover, this would create bacteria-like nanoarchitectures that could be recognized by the host in a way similar to the pathogenic agent but exploiting the optimal particle size to elicit immune system activation at the tumor and lymph nodes.

The immunosuppressive environment of the tumor has proven to be a major obstacle for ligands targeting the TLR4 signaling pathway to be effective in anti-tumor vaccination. The clinical efficacy of checkpoint inhibition on the other hand is limited by requiring the existence of antitumor CD8<sup>+</sup> T cells at the tumor before the checkpoint immunotherapy, with only certain tumors being immunogenic enough to generate a natural antitumor T-cell response. Moreover, even once this natural T-cell response is elicited, cancer cells may undergo a series

of genetic and nongenetic processes to avoid being eliminated by the immune system and to acquire resistance to immune checkpoint blockade.<sup>[6]</sup> Insufficient generation of antitumor T cells, inadequate function of tumor-specific T cells, impaired formation of T-cell memory and cancer immunoeediting all contribute to monotherapy with checkpoint inhibition being ineffective in most cases.

To date, the most effective immune checkpoint inhibitors are monoclonal antibodies that bind to either programmed death-1 (PD-1) or to its ligand PD-L1.<sup>[42]</sup> The PD-1 receptors expressed on activated T cells, on binding to PD-L1, induce a state of ineffective T-cell activity. Hence, PD-L1 expression on tumor cells confers a potent escape mechanism from the host T-cell immunity. Since the induction of PD-L1 on DCs by TLR ligation has been reported for some TLR agonists and shown to be a mechanism limiting the antitumor efficacy of TLR agonists,<sup>[13,43,44]</sup> we reasoned that blocking the immunosuppressive roles of PD-L1 expression by the tumor would significantly improve the efficacy of the vaccination. Moreover, the induction of PD-L1 is linked with the induction and maintenance of  $T_{\text{regs}}$  cells,<sup>[45,46]</sup> which are immunosuppressive and increased in cancer patients. Thus, blocking one inhibitory factor of PD-L1 may decrease other inhibitory factors. To investigate the efficacy of the cancer vaccines and nanovaccines and potential synergism with PD-L1 checkpoint inhibition arising from the functional contributions of tumor cell PD-L1 expression,<sup>[47]</sup> we previously used CRISPR/Cas9 genome-editing technology delivered within lentiviral particles to abrogate PD-L1 expression only in the tumor cells.<sup>[48,49]</sup>

Here, we have developed a nanovaccine featuring a model antigen (OVA) linked to mIONPsp by hydrazone bonds, and an adjuvant (Xcc LOS) adhered to the mIONPsp by hydrophobic interactions to create pathogen-mimicking nanostructures. The protective effect of the OVA linked to mIONPsp via hydrazone bond (mIONPsp-HyNic-FB-OVA) formulated with the pathogen-mimicking mIONPsp-Xcc LOS as adjuvant was investigated in vitro and in mice against B16-F10 melanoma expressing OVA. The results provide the first evidence that the LOS from Xcc can elicit antitumor immune responses and showed that delivery of Xcc LOS by mIONPsp improves the immunostimulatory properties and promotes reduced cytotoxicity. Furthermore, the abrogation of PD-L1 on the tumor cells massively improved the effect of vaccination, which conferred 100% long-term immune protection against multiple tumor challenges.

## 2. Results and Discussion

### 2.1. Assembly of Pathogen-Mimicking TLR4 Agonist-Functionalized NP Micelles

The encapsulation of hydrophobic IONPsp, QDs, and IONPc (cubic iron oxide nanoparticles) in PEG phospholipids with incorporation of the two different TLR4 agonists, Xcc LOS (a lipooligosaccharide derived from *Xanthomonas campestris*, a plant pathogen) and *E. coli* LOS (a lipooligosaccharide from *Escherichia coli*) provided micelles that could be stored in an aqueous solution for weeks without major aggregation and



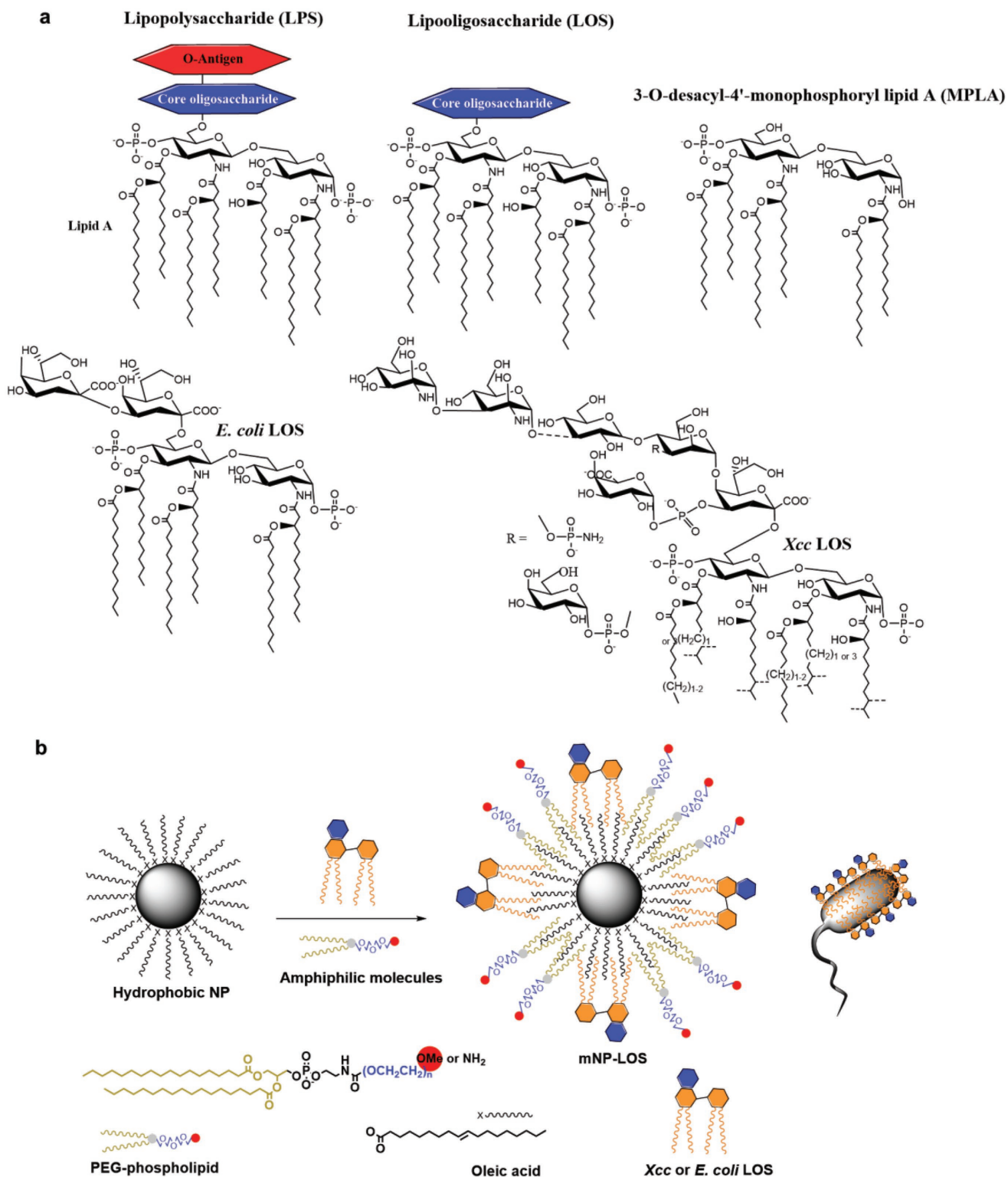


**Figure 1.** a) Chemical structures of the TLR4 agonists and b) schematic of the self-assembly process for the synthesis of the water-soluble and pathogen-mimicking nanoparticles (NP micelles (mNP) incorporating *Xcc* or *E. coli* LOS molecules).

size changes. In contrast, the incorporation of MPLA immediately afforded insoluble aggregates. The phospholipid-PEG and the TLR4 agonists are amphiphilic molecules, which to

reduce NP/water surface tension associate with the surface of the original hydrophobic NPs through interdigitation of their acyl chains by van der Waals attractive interactions and create

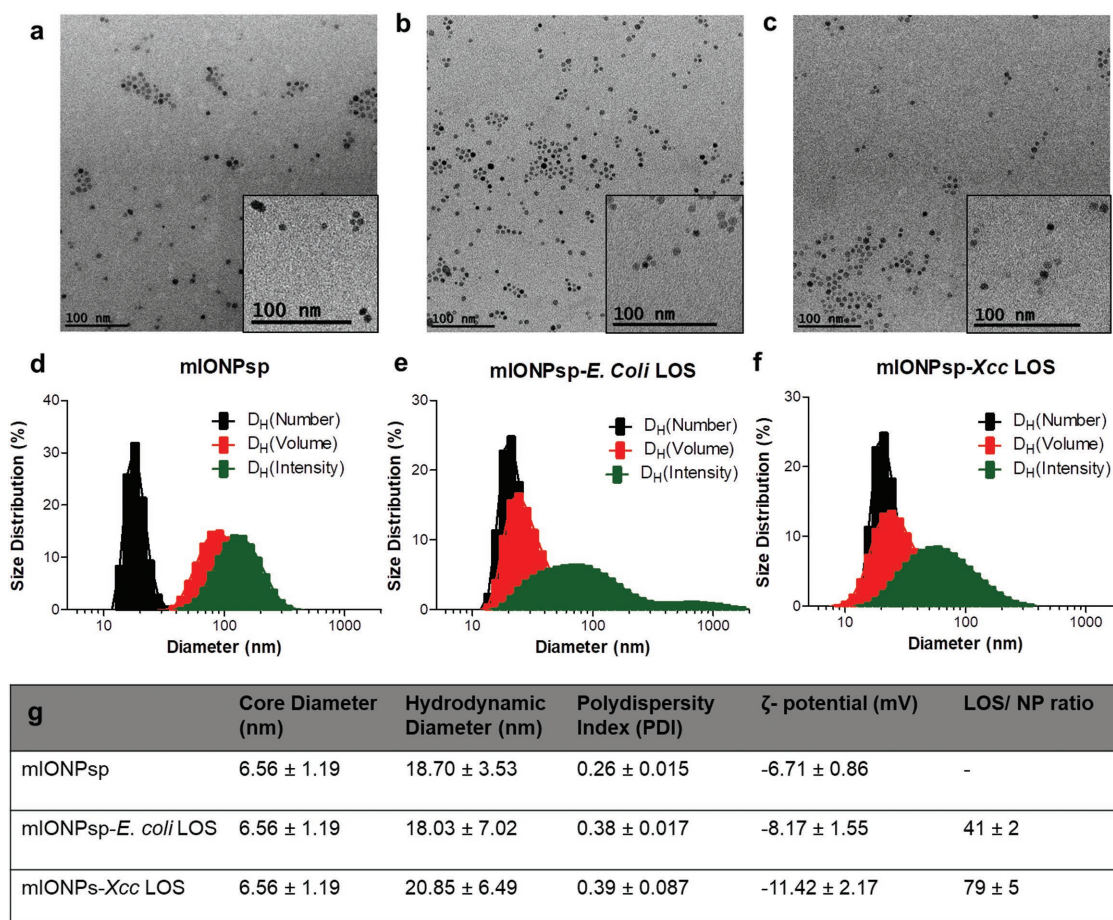


**Figure 2.** Size and Z-potential of mIONPsp with and without LOS incorporation. a–c) TEM images and d–f) DLS analysis. g) Main characterization data: IONP core diameter from TEM images and counting more than 200 nanoparticles, number-average hydrodynamic diameter and polydispersity index obtained by DLS, Z-potential and number of biomolecules per IONP (bottom) based on  $n > 10$  formulation replicates.

the self-assembled bacteria-like nanoarchitectures. The organization of hydrophilic components/precursors at the surfactant/water interface through electrostatic and hydrogen bonding interactions resulted in encapsulation of the NPs in a shell formed by the polar head groups, making the pathogen-mimicking NP-filled micelles (mNPs) soluble and stable in water (Figure 1b). For MPLA, the lack of the hydrophilic O-antigen polysaccharide and core oligosaccharide chain might make the micelle surface less hydrophilic and increase the surface hydrophobicity, which promotes the formation of insoluble large aggregates. To remove NP-free micelles, the samples were centrifuged (three cycles), the supernatants were kept for quantification of LOS and *Xcc* LOS loading (see below) and the pelleted mNPs were redissolved in aqueous solution. The lipooligosaccharide-free mNPs prepared as controls and the pathogen-mimicking mNPs incorporating the TLR4 agonists were characterized by transmission electronic microscopy (TEM), dynamic light scattering (DLS), and by measuring the Z-potential of the particles (Figure 2 and Figures S1 and S2, Supporting Information). The size distribution of bacteria-like TLR4 agonist-functionalized mNPs is in the ideal range (20–100 nm) for lymphatic delivery (with a number-averaged hydrodynamic diameter of  $\approx 20$  nm for IONPsp and QDs and of  $\approx 70$  nm for

IONPsp with size polydispersity index between 0.16 and 0.39) and they showed a more negative Z-potential than the drug-free controls. This result is consistent with the high negative charge density of the LOS molecules provided by the phosphate, carboxylate, and phosphoramidate groups. Also consistent with their different structures, the bacteria-like mNPs functionalized with *Xcc* LOS (mIONPsp-*Xcc* LOS) had a more negative surface charge ( $-11.42 \pm 2.17$  mV) than mNPs functionalized with *E. coli* LOS ( $-8.17 \pm 1.55$  mV). Apart from an optimum size of 20–100 nm, their negative surface charge provides additional advantages for lymph node targeting. Thus, electrostatic repulsion with the negatively charged interstitial matrix allows the negatively charged particles to move faster through the interstitium and be more efficiently accumulated in the draining lymph nodes.<sup>[50,51]</sup>

Studies have shown also that hydrophobicity facilitates both uptake by antigen presenting cells and delivery to lymph nodes.<sup>[50,52,53]</sup> In these constructs bound LOS and the oleic acid chains of the NPs provide hydrophobic components to the micelle, which upon exposure to the surface can facilitate interaction with the membrane of the antigen presenting cells. The mIONPsp-LOS therefore possess all the key features of materials that can effectively target the lymph nodes, namely a size

of 20–100 nm, a negative surface and an appropriate level of hydrophobicity.

To quantitate TLR4 agonist loading, we carried out two sets of experiments. After pelleting the mNP-LPS/LOS systems by three cycles of centrifugation, IL-6 cytokine production in the macrophage cell line J774A.1 after incubation with the supernatants was compared with the dose-response curves obtained with the corresponding LOS. Since the limulus amoebocyte lysate (LAL) test is an FDA-approved assay for the determination of endotoxin in medicines, biological products and medical devices, and has been used to detect endotoxin contamination in nanomaterials,<sup>[54]</sup> the quantification of LPS in the supernatants was also determined by an endpoint chromogenic LAL assay. Both assays produced essentially identical results (Figure S3, Supporting Information). The results showed that the *Xcc* LOS is incorporated better than the *E. coli* LOS in the mIONPsp and mIONPc ( $76 \pm 6\%$  vs  $22.2 \pm 5.1\%$  and  $44 \pm 11\%$  vs  $25 \pm 9\%$ , respectively, Figure S4, Supporting Information). The mIONPsp could be loaded with  $79 \pm 5$  and  $41 \pm 2$  molecules of *Xcc* LOS and *E. coli* LOS per particle, respectively (Figure 2g). The larger NP core size of the mIONPc allowed to increase the loading to  $240 \pm 26$  *Xcc* LOS molecules/particle and  $76 \pm 7$  molecules of *E. coli* LOS/particle (Figure S2g, Supporting Information). Both types of nanoparticles are stabilized with an oleic acid/oleylamine surfactant layer. In contrast, the commercial QDs with a similar core size to the mIONPsp showed preference for incorporating *E. coli* LOS over *Xcc* LOS ( $29 \pm 1$  *Xcc* LOS molecules/particle vs  $155 \pm 11$  molecules of *E. coli* LOS/particle). This result may reflect the differences in the hydrophobic chains, where specific chain lengths etc. contributed to forming more extensive van der Waals interactions with the surfactants stabilizing the NPs. Silipo et al. determined the complete structure of *Xcc* LOS and it was found to be a unique molecule with high negative charge and variability in the fatty acid length and possessing an uncommon symmetric (3 + 3) distribution of acyl chains on the disaccharide backbone with the acyloxyacyl groups exclusively ester-linked.<sup>[55,56]</sup>

To study the behavior of the mIONPsp-*Xcc* LOS over time, the size of these constructs was analyzed immediately after purification and over a 4 week period in  $10 \times 10^{-3}$  M PBS. Although the results showed some aggregation the size of the mIONPsp-*Xcc* LOS over time was still within the ideal range for reaching the lymph nodes (Figure S5, Supporting Information). To study the release of *Xcc* LOS molecules, at designed time points (week 0, 1, and 2)  $10 \times 10^{-3}$  M PBS solutions of the mIONPsp-*Xcc* LOS were subjected to centrifugation and the amount of *Xcc* LOS in the supernatant was determined as described below. The results showed that only 5% of the *Xcc* LOS molecules are released. In the outer membrane of gram negative bacteria the negatively charged LPS molecules cover most of the outer surface and divalent cations such as  $Mg^{2+}$  and  $Ca^{2+}$  are essential to neutralize this negative charge and allow strengthening of the lateral interactions between neighboring LPS molecules, which provides enhanced stability for the external bacterial membrane.<sup>[54,57,58]</sup> Similar electrostatic interactions and effects such as increased hydrogen bonding and tighter lipid packing and cross-linking exerted by divalent cation bridging can be expected to take place in the pathogen-mimetic mNP-LOS nanostructures to provide the observed stability.

## 2.2. Synthesis and Characterization of OVA Linked to mIONPsp via Hydrazone Bond (mIONPsp-HyNic-OVA)

Several studies have improved the immunogenicity of antigens by nanoparticle delivery using *N*-hydroxysuccinimide and 1-ethyl-3-(3-dimethylaminopropyl) carbodiimide coupling chemistry for the bioconjugation.<sup>[21,26,59]</sup> Other studies have used reductively labile disulfide-based antigen conjugation.<sup>[60]</sup>

Here, the mIONPsp-antigen conjugates were developed by the means of biorthogonal chemistry and hydrazone ligation. The bis-aryl-hydrazone-linking conjugation strategy is shown in Figure 3a and offers high chemoselectivity, high yields at low concentrations, enhanced reaction rates at pH 7 ( $k_{on} = 170 \text{ M}^{-1} \text{ s}^{-1}$  in the presence of  $100 \times 10^{-3}$  M aniline) and easy reaction monitoring. To introduce the required functional groups onto the mIONPsp, the terminal amine of the mIONPsp prepared using 1,2-distearoyl-sn-glycero-3-phosphoethanolamine-*N*-[amino(polyethylene glycol)-2000] (DSPE-PEG-amine) was modified to an aromatic hydrazone by reaction with the activated ester of the linker succinimidyl 6-hydrazinonicotinate acetone hydrazone (S-HyNic). The HyNic-modified mIONPsp (mIONPsp-HyNic) were purified by a desalting column and spin filtration. The average molar substitution ratio of the mIONPsp with the HyNic linker was  $\approx 10$ , which was determined by reacting mIONPsp-HyNic with 4-nitrobenzaldehyde and measuring the formation of the bis-aryl hydrazone bond at 345 nm. Lysine residues of OVA were modified to an aromatic aldehyde by reacting it with the activated ester of the linker succinimidyl 4-formylbenzoate (4FB) and purified by a desalting column and spin filtration. The substitution ratio of the OVA with the 4FB linker was determined by reaction with 2-hydrazinopyridine-2HCl and measuring the formation of the bis-aryl hydrazone at 350 nm, and was 2–3 molecules of 4FB per OVA (Figure 3b). The ligation reaction of the aromatic aldehyde functionalized 4FB-OVA ( $20\text{--}30 \times 10^{-6}$  M) with hydrazine activated mIONPsp-HyNic ( $0.5\text{--}3 \times 10^{-6}$  M IONPs) carried out at pH 6.2 and monitored by the hydrazone chromophore formation achieved a high level of conjugation ( $\approx 85\text{--}90\%$ ) in 2 h and 80% conversion already within the first 10 min of the reaction in the presence of  $100 \times 10^{-3}$  M aniline catalyst (Figure 3c). Quantitative analysis of protein content by BCA showed conjugation of 6 molecules of OVA per IONPsp. TEM and DLS studies confirmed that this conjugation strategy preserves the 20–100 nm size for lymph node targeting (Figure 3d,e), and that the mIONPsp-HyNic-4FB-OVA are stable for weeks in PBS (Figure 3f,g).

## 2.3. mNP Modulates the Immunostimulatory Properties and Cytotoxicity of the TLR4 Agonists

Many studies have shown that the chemical structure dictates the immune response to LPS. Moreover, some studies suggest that LPSs as amphiphilic molecules form supramolecular aggregates in aqueous environments, and that these structures are the biologically active units of LPS.<sup>[61]</sup> However, the type of supramolecular aggregate structures formed also depends strongly on the chemical structure of the LPS molecules.



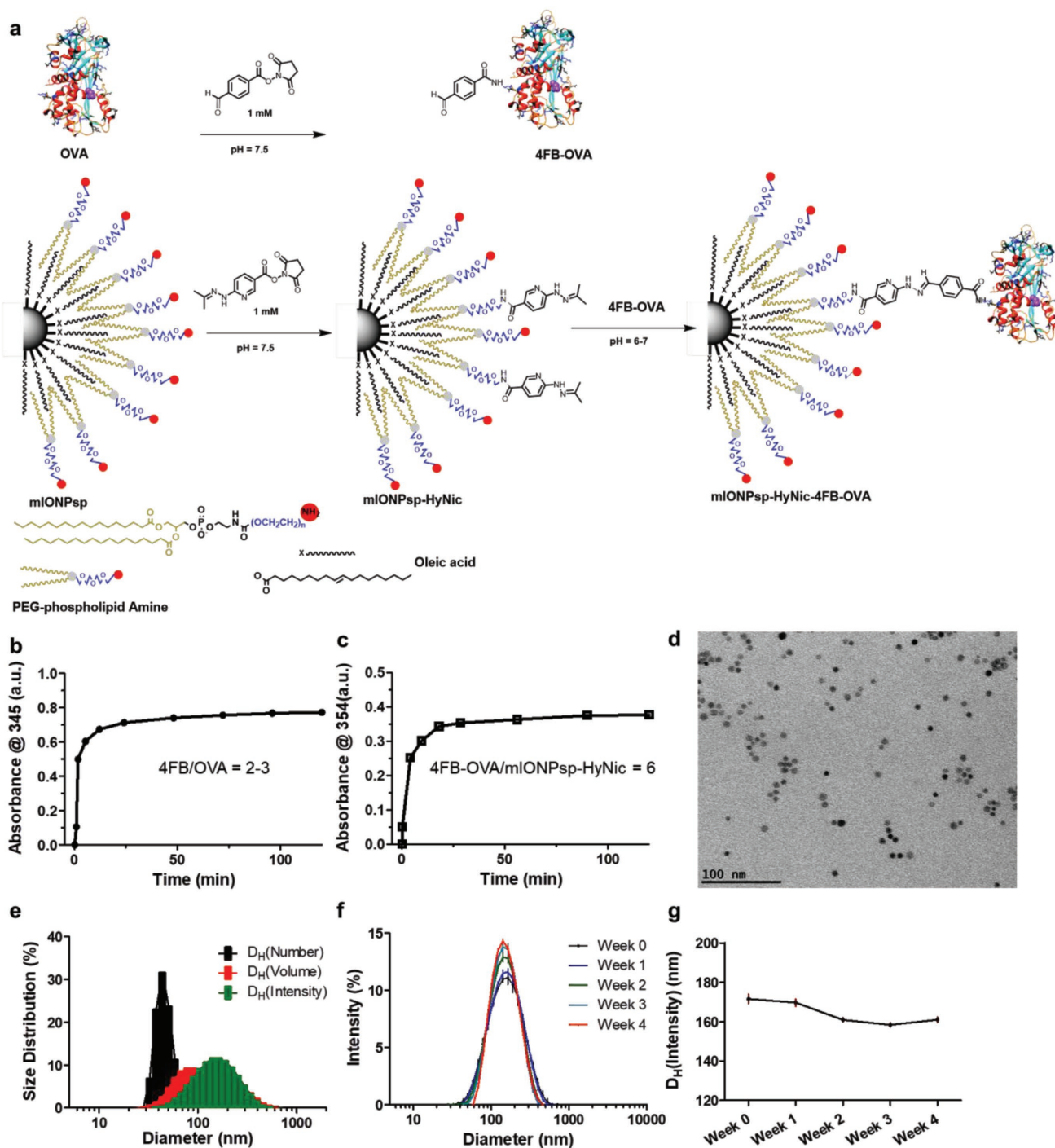


**Figure 3.** a) General strategy for the conjugation of the antigen (OVA) to mIONPsp. b,c) UV monitoring of the chemical ligations. b) The substitution ratio of the OVA with the 4-FB linker was determined by reaction of the FB-OVA with 2-hydrazinopyridine-2HCl. c) The formation of the 4FB-modified OVA and the ligation reaction of 4FB-OVA ( $20\text{--}30 \times 10^{-6}$  M) to mIONPsp-HyNic ( $0.5\text{--}3 \times 10^{-6}$  M mIONPsp) in presence of  $\approx 100 \times 10^{-3}$  M of aniline. d–g) Size and stability of mIONPsp-HyNic-4FB-OVA. Representative d) TEM micrograph and e–g) DLS analysis of size and size distribution over time.

Incorporation into mNPs ensures the formation of supra-molecular structures where multiple copies of the LPS molecules are clustered, and therefore we reasoned they would show equal or even to be more active than the mNP-free preparations. When stimulating the macrophage cell line J774A.1 with the different TLR4 ligands in vitro to produce IL-6, the

biological activity of *E. coli* LPS showed greater IL-6 production in comparison to equal amounts of *E. coli* LOS or *Xcc* LOS, and lower cell viability. Comparison of IL-6 production and cell viability of the TLR4 ligands compared to TLR4 ligand loaded mNPs showed that the immunostimulatory properties and cytotoxicity are modulated by each of the mNPs differently.



Incorporation into mIONPsp enhanced IL-6 production and significantly reduced cytotoxicity for *Xcc* LOS (Figure S6a,b, Supporting Information). In contrast, *E. coli* LOS incorporation into mIONPc lead to reduced IL-6 production and significantly increased cytotoxicity (Figure S7, Supporting Information). The mQDs enhanced IL-6 production without affecting cytotoxicity (Figure S8, Supporting Information).

On the basis of these results, we selected for further studies the mIONPsp-*Xcc* LOS system.

Since dendritic cells are the key initiators and modulators of the adaptive immune response, the immunostimulatory activity was also tested in primary murine bone-marrow-derived dendritic cells (BMDCs). The results showed *Xcc* LOS and mIONPsp-*Xcc* LOS to be as effective as *E. coli* LPS and MPLA at inducing IL-6, IL-12, and TNF- $\alpha$  release and increasing the expression of costimulatory molecules CD80 and CD86, and that the mIONPsp alone also have some ability to activate DCs (Figure S6c,d, Supporting Information). Moreover, the results confirm that when DCs are confronted with the TLR4 agonists, inhibitory immune pathways can be triggered. The different TLR4 agonists, mIONPsp-*Xcc* LOS and mIONPsp significantly upregulated the expression of the inhibitory molecules PD-L1 in DCs (Figure S6d, Supporting Information), which is indicative of the potential for synergy between the vaccines and PD-L1 checkpoint inhibition. The results also showed that mIONPsp-*Xcc* LOS and mIONPsp-HyNic-4FB-OVA are essentially nontoxic to DCs (Figure S9, Supporting Information).

#### 2.4. mIONPsp-*Xcc* LOS and mIONPsp-HyNic-4FB-OVA Reach Endosomal Compartments

TLR4 is unique, in that it is the only TLR that activates both the MyD88- and TRIF-dependent pathways.<sup>[62]</sup> LPS binding to TLR4 induces MyD88- and TRIF-dependent pathways from the plasma membrane and endosomes, respectively. It has been shown that after TLR4 encounters LPS, endosomes showing LPS and TLR4 colocalization appear within 15 min.<sup>[63]</sup> To enable tracking of the mIONPsp during cellular uptake a 5% rhodamine B-labeled phospholipid was incorporated during the micelle synthesis. As expected, the mIONPsp(Rho)-*Xcc* LOS and mIONPsp(Rho)-HyNic-4FB-OVA colocalized with lysosomes in the J774A.1 cells (Figure 4).

#### 2.5. OVA Antigen Delivered by mIONPsp-HyNic-4FB-OVA and Formulated with the Pathogen-Mimicking mIONPsp-*Xcc* LOS Provides Enhanced Protection against B16-F10(OVA) Melanoma Tumors

B16-F10 melanomas have been widely used as a poorly immunogenic, highly aggressive model for murine tumor immunotherapy studies. To investigate the efficacy of *Xcc* LOS as adjuvant evaluating antigen-specific responses, we used the B16-F10 sub-line engineered to express the model antigen ovalbumin (B16-F10(OVA)). To the best of our knowledge, the adjuvant properties of *Xcc* LOS for vaccine development and immunotherapy have not

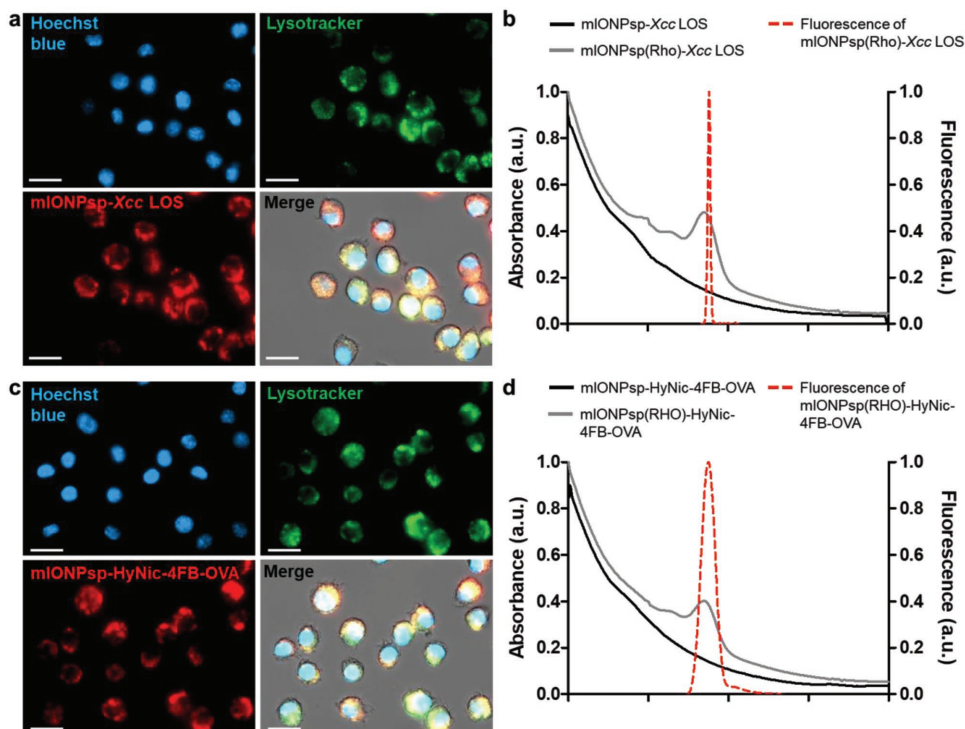


**Figure 4.** In vitro uptake and trafficking of rhodamine labeled mIONPsp-*Xcc* LOS and mIONPsp-HyNic-4FB-OVA micelles. a,c) Fluorescence microscopy images of J774A.1 macrophages showing endocytic uptake of a) mIONPsp-*Xcc* LOS and c) mIONPsp-HyNic-4FB-OVA after 3 h incubation. Cells' nuclei were stained with Hoechst blue and lysosomes and endosomes with lysotracker green. b,d) UV-vis absorption and fluorescence spectrum of b) rhodamine-labeled mIONPsp-*Xcc* LOS and d) mIONPsp-HyNic-4FB-OVA. Scale bar =  $20 \times 10^{-6}$  m.

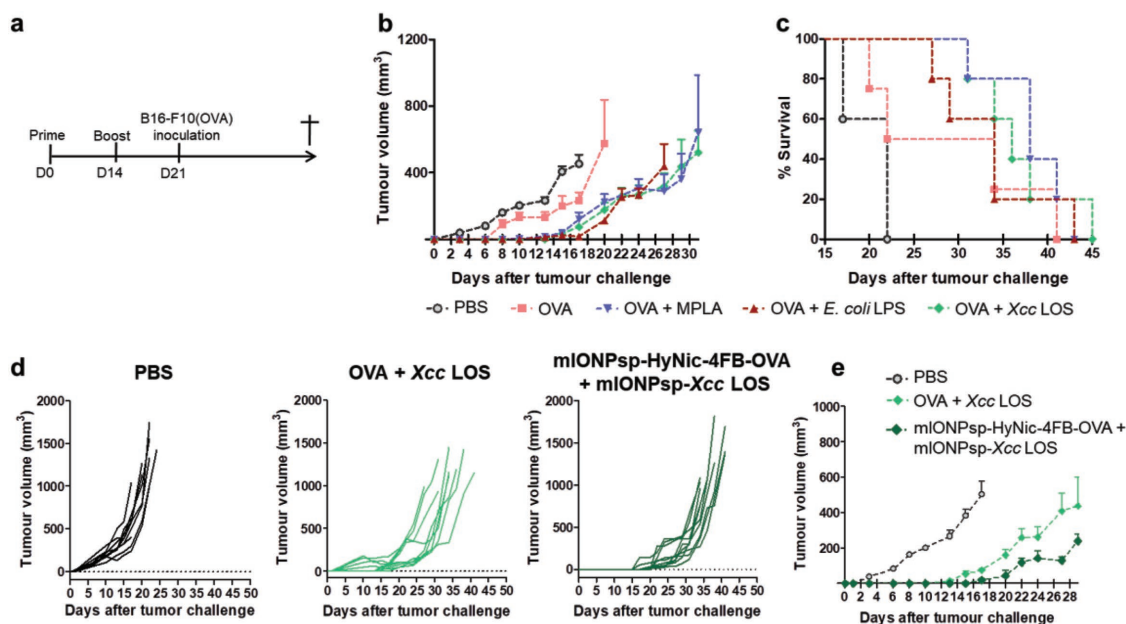


**Figure 5.** Protective immunity against B16-F10(OVA) melanoma cells by the use of the different TLR4 agonist adjuvants coadministered with tumor antigen. a) Vaccination scheme. C57BL/6 mice were s.c. immunized with the indicated formulations (5  $\mu$ g of OVA, 1  $\mu$ g of TLR4 agonist per mouse, 25–70  $\mu$ g of IONP on day 0 and 14 and s.c. challenged with  $3 \times 10^5$  B16-F10(OVA) cells per mouse on day 21. b–e) Average and individual tumor growth curves and Kaplan–Meier survival curves. The data show mean  $\pm$  SEM from a representative experiment ( $n = 5–10$ ) from 2 to 3 independent experiments.

been investigated previously. Hence, for comparison of adjuvant properties, C57BL/6 mice were immunized subcutaneously (s.c.) with OVA (5  $\mu$ g) alone or with OVA (5  $\mu$ g) + *E. coli* LPS (1  $\mu$ g), OVA (5  $\mu$ g) + MPLA (1  $\mu$ g), and OVA (5  $\mu$ g) + *Xcc* LOS (1  $\mu$ g) at days 0 and 14, and at day 21 week were challenged with  $3 \times 10^5$  B16-F10(OVA) cells, and tumor growth was monitored until they reached the limits of the established endpoint (Figure 5a). To evaluate the utility of the nanoparticle delivery, another group of mice was immunized with mIONPsp-HyNic-4FB-OVA formulated with pathogen-mimicking mIONPsp-*Xcc* LOS as adjuvant. All animals vaccinated with the TLR4 agonists showed reduced tumor growth and provided survival benefits (median survivals of 34–38 d) compared to the OVA-treated (median survival of 28 d) even with the low adjuvant doses (1  $\mu$ g). Notably, despite a weaker capacity of *Xcc* LOS to induce IL-6 production in the J774A.1 macrophages, it proved to be as effective as adjuvant as the strong TLR4 ligand *E. coli* LPS and the clinically approved MPLA (Figure 5b,c). Compared to the nanoparticle-free treatments, the immunization with mIONPsp-HyNic-4FB-OVA formulated with pathogen-mimicking mIONPsp-*Xcc* LOS delayed longer the tumor growth (Figure 5d,e).

We investigated the immune mechanisms behind the enhanced antimelanoma response to the nanovaccines. To this end, systemic antibody responses as well as the induction of tumor antigen-specific cytotoxic T lymphocyte (CTL) effector and memory response were assessed. Blood samples were obtained and the production of OVA-specific IgG, IgG1, and IgG2 antibodies in the circulation was evaluated by ELISA. The results showed that the TLR4 agonists elicited higher levels of antibodies specific for OVA than immunization with antigen alone (Figure 6a). In particular, we observed the induction of the IgG2c isotype, which is typically implicated with enhanced protection

in both infectious diseases and cancer and is not induced by the clinically approved aluminum adjuvants. Notably, mIONPsp-HyNic-4FB-OVA formulated with mIONPsp-*Xcc* LOS elicited similar or lower levels of total IgG, IgG1, and IgG2c antibodies than the vaccines without mIONPsp vehicles. Although the increase in titers of antigen-specific antibodies in these immunizations indicates immune adjuvant activity in these preparations, it does not explain the enhanced protection against the melanoma challenge provided the mIONPsp-based nanovaccines.

Contrasting with vaccination strategies aimed at generating antibody production, generating protective memory CD8<sup>+</sup> T-cells has proven more difficult to achieve.<sup>[64]</sup> We therefore analyzed if the immunization with OVA + *Xcc* LOS and mIONPsp-HyNic-4FB-OVA formulated with pathogen-mimicking mIONPsp-*Xcc* LOS was able to drive antigen-specific CD8<sup>+</sup> T-cell responses. For this, we monitored the frequency of OVA<sub>257-264</sub> (SIINFEKL)-specific CD8<sup>+</sup> T-cells by H-2Kb/SIINFEKL dextramer staining and flow cytometric analysis. The highest frequency of SIINFEKL-specific CD8<sup>+</sup> T-cells was found in mice immunized with OVA antigen delivered by mIONP-HyNic-4FB-OVA and formulated with pathogen-mimicking mIONPsp-*Xcc* LOS (Figure 6b).

Following infection or vaccination, naive CD8<sup>+</sup> T cells are primed in secondary lymph node by DCs and consequently proliferate and differentiate into effector and memory cells. The CD8<sup>+</sup> memory T-cells divide into “effector memory” cells (T<sub>EM</sub>) and “central memory” (T<sub>CM</sub>) cells. T<sub>EM</sub> and T<sub>CM</sub> exhibit distinct functional abilities,<sup>[65]</sup> which intriguingly could potentially be generated differently in response to the vaccines and nanovaccines and play a role in their different protective abilities. Whereas T<sub>EM</sub> are localized in peripheral nonlymphoid tissues (e.g., lung, liver, intestine), spleen, and blood and can

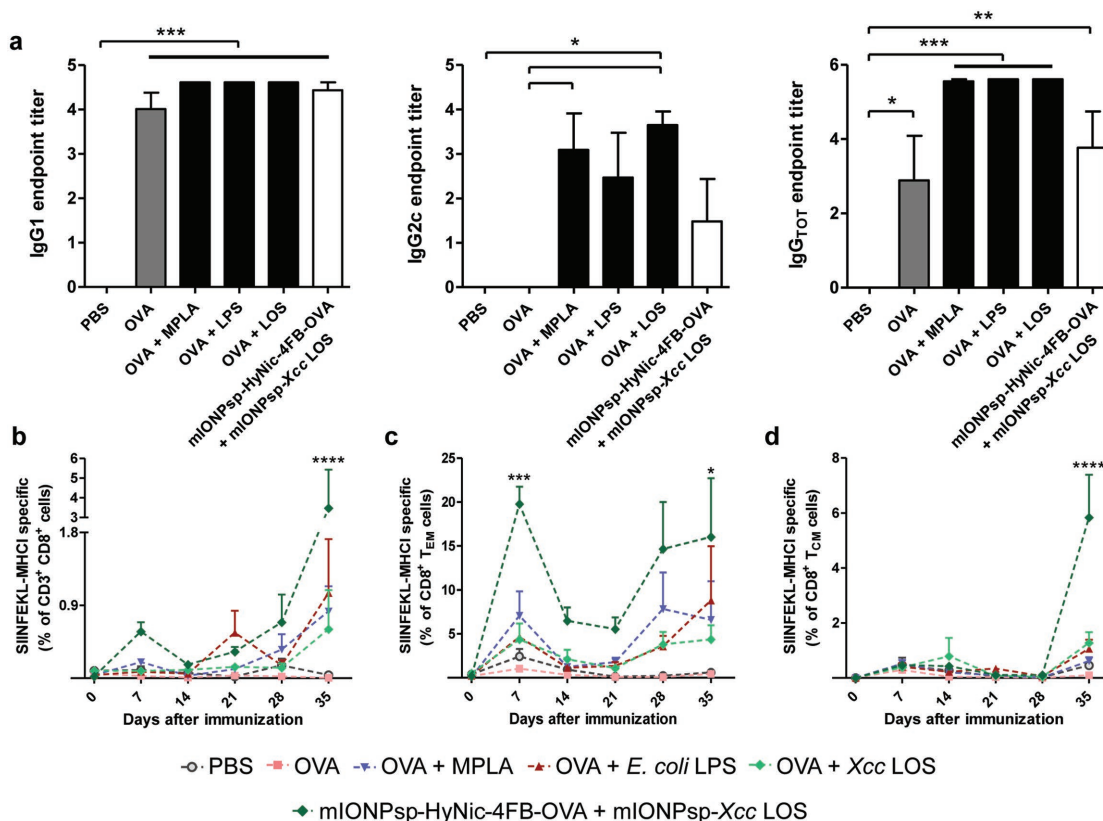


**Figure 6.** Immunization with the mIONPsp-based vaccines triggers a higher-level tumor antigen-specific cytotoxic T lymphocyte (CTL) effector responses. a) OVA-specific serum IgG1, IgG2c, and total IgG titers 2 weeks after s.c. challenge with  $3 \times 10^5$  B16-F10(OVA) cells (day 35). b) Analysis of frequency of circulating OVA<sub>257-264</sub> (SIINFEKL)-specific CD8<sup>+</sup> T-cells isolated from blood. c,d) Frequency of SIINFEKL-specific CD8<sup>+</sup> T<sub>EM</sub> and T<sub>CM</sub> cells. T<sub>CM</sub> cells are defined as CD3<sup>+</sup>CD8<sup>+</sup>CD62L<sup>+</sup>CD44<sup>+</sup> and T<sub>EM</sub> as CD3<sup>+</sup>CD8<sup>+</sup>CD62L<sup>+</sup>CD44<sup>+</sup>. Data presented as mean  $\pm$  SEM.  $n = 5$  mice per group. \*\*\*\* $P < 0.0001$ , \*\*\* $P < 0.001$ , \*\* $P < 0.01$ , \* $P < 0.05$  by a) one-way ANOVA followed by Tukey's test and b–d) two-way ANOVA followed by Bonferroni's test.

immediately recognize and kill the target virally infected/cancer cells, T<sub>CM</sub> cells are known to be able to traffic into lymph nodes directly from the blood and are thought to provide a sustained and robust CTL recall response to control subsequent disease challenges.

We analyzed the frequency of circulating SIINFEKL-specific CD8<sup>+</sup> T<sub>EM</sub>-cells (CD44<sup>+</sup>CD62L<sup>low</sup>) and T<sub>CM</sub>-cells (CD44<sup>+</sup>CD62L<sup>high</sup>) over time ( $t = 0, 7, 14, 21, 28,$  and  $35$  d). mIONPsp-vaccinated mice had much greater frequency of both antigen-specific T<sub>EM</sub> and T<sub>CM</sub> cells. The T<sub>EM</sub> population peaked at day 7 after the first vaccination and the levels increased drastically on day 35, i.e., after boost and tumor challenge (Figure 6c). The highest frequency of the SIINFEKL-specific CD8<sup>+</sup> T<sub>CM</sub>-cells was observed on day 35 (Figure 6d). The results demonstrate that the nanovaccines generate more effectively protective memory CD8<sup>+</sup> T cells.

## 2.6. The Adjuvant Properties of Xcc LOS Enhanced by Nanoparticle Delivery Confers 100% Protection against the B16-F10(OVA) Melanoma Cells When PD-L1 Expression is Abrogated in Tumor Cells

We next explored the effect of immunization combined with immune checkpoint inhibition at the level of the cancer cell

using B16-F10(OVA) melanoma cells with silenced PD-L1. PD-L1 blockade achieves the same effects than knocking out PD-L1 in cancer cells as demonstrated previously. We used a protocol that uses CRISPR/Cas9 genome editing and lentiviral particles to generate the PD-L1-deficient B16-F10(OVA), as described before;<sup>[48,49]</sup> the abrogation of PD-L1 was confirmed by flow cytometry (Figure S10, Supporting Information). This genetically modified cell line, B16-F10(OVA)  $\Delta$ PD-L1, was used in the prophylactic immunization assay (Figure 7a). C57BL/6 mice were subcutaneously administered PBS or were vaccinated with OVA + Xcc LOS and mIONPsp-HyNic-4FB-OVA + mIONPsp-Xcc LOS (days 0 and 14) and inoculated with  $2 \times 10^6$  B16-F10(OVA)  $\Delta$ PD-L1 cells (day 21). All the mice treated with PBS developed melanoma tumors within 10 d. As PD-L1 abrogation decreases tumor cell growth, we first confirmed that the tumor growth kinetics following inoculation of  $2 \times 10^6$  B16-F10(OVA)  $\Delta$ PD-L1 and inoculation of a lower dose ( $3 \times 10^5$ ) of B16-F10(OVA) cells was equivalent for mice treated with PBS. However, in the case of mice immunized with OVA + Xcc LOS, mice remained tumor free for 20 d and 40% did not develop tumor past 100 d after the challenge with B16-F10(OVA)  $\Delta$ PD-L1 cells, compared to all the mice developing tumor by day 20 after the challenge with the B16-F10(OVA) cells. In the case of mice immunized with mIONPsp-HyNic-4FB-OVA + mIONPsp-Xcc LOS 100% of the animals were free of tumor

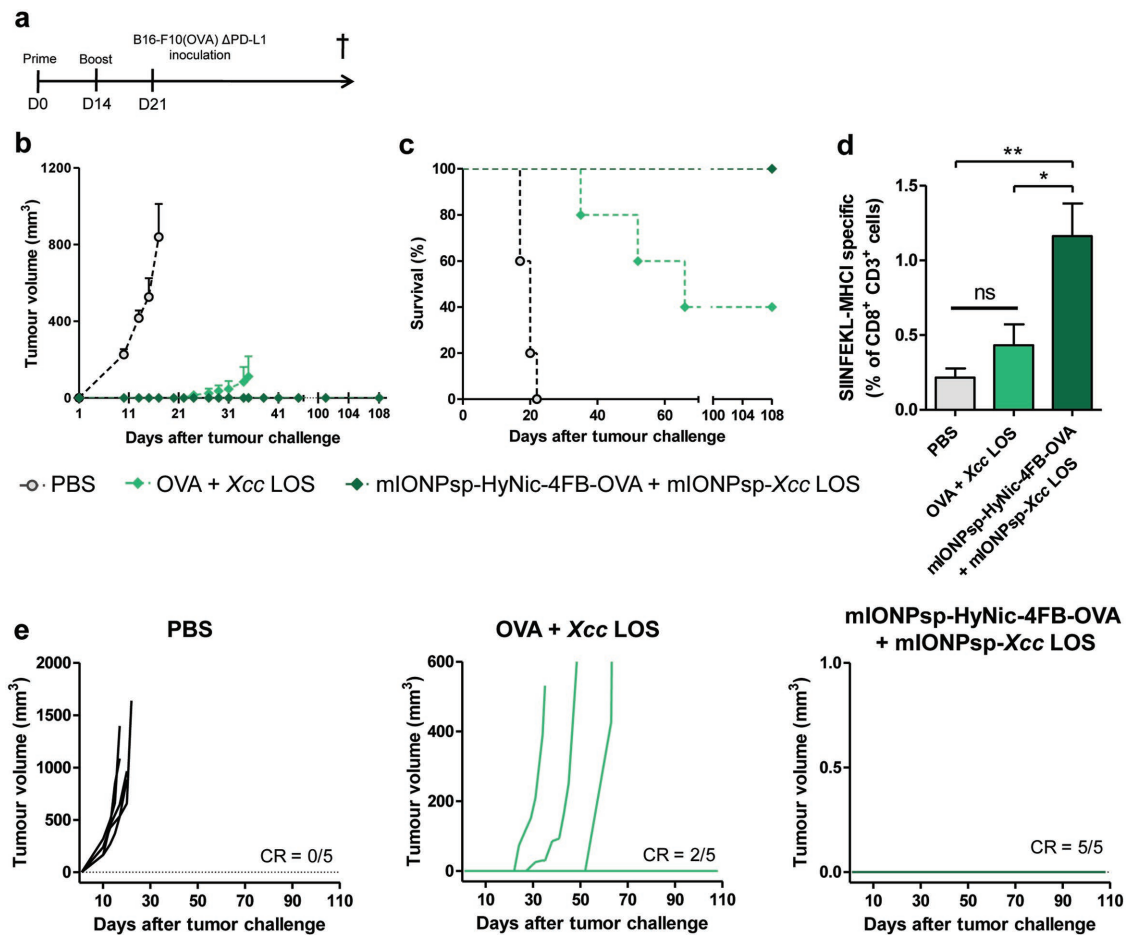


**Figure 7.** Protective immunity against B16-F10(OVA) melanoma cells with knocked-down expression of PD-L1 (B16-F10(OVA)  $\Delta$ PD-L1). a) Vaccination scheme. C57BL/6j mice ( $n = 5$ ) were s.c. challenged with  $2 \times 10^6$  B16-F10(OVA)  $\Delta$ PD-L1 cells 7 d after the last vaccination with 5  $\mu$ g of OVA, 1  $\mu$ g Xcc LOS per mouse, 25  $\mu$ g of IONP). b) Average and e) individual tumor growth curves and c) Kaplan–Meier survival curves. d) Circulating SIINFEKL-specific CD8<sup>+</sup> T cells 35 d after the first immunization (2 weeks after tumor inoculation). \*\* $P < 0.01$ , \* $P < 0.05$ , ns, nonsignificant by one-way ANOVA followed by Tukey’s test. CR, fraction of complete tumor rejection.

110 d after the challenge with B16-F10(OVA)  $\Delta$ PD-L1 cells (Figure 7b,c,e). Furthermore, analysis of SIINFEKL-specific CD8<sup>+</sup> T cells corroborated the enhanced protection against the melanoma cells (Figure 7d). Hence mIONPsp delivery combined the permanent PD-L1 checkpoint blockade remarkably improved the efficacy of the vaccination.

To assess the longevity and efficiency of memory recall responses in the mIONPsp-vaccinated mice, we investigated the immune responses 100 d after the boosting immunization. Mice received a recall immunization 103 d after the boost and the capacity to clear a rechallenge ( $2 \times 10^6$  B16-F10(OVA)  $\Delta$ PD-L1 cells s.c. implanted on the right back on day 122) was investigated. Whereas the control mice developed melanoma tumors within 10–15 d, 100% of the mIONPsp-vaccinated mice remained tumor-free until the end of the experiment (day 139) (Figure 8b). We analyzed the frequency of circulating SIINFEKL-specific CD8<sup>+</sup> T cells in the blood previous to the recall immunization. We did not detect SIINFEKL-specific cells neither within the CD8<sup>+</sup> nor in the T<sub>CM</sub> cell population, comparing immunized mice with mice of the same age that had not been immunized/challenged with the melanoma cells.

However, analysis of the T<sub>EM</sub> subset revealed that mice immunized with mIONPsp-HyNic-4FB-OVA + mIONPsp-Xcc LOS had high levels of SIINFEKL-specific CD8<sup>+</sup> T<sub>EM</sub> cells even 100 d after the first immunization (Figure 8c). To analyze the magnitude and quality of the memory response generated after the recall, we analyzed the frequency of circulating antigen-specific T cells. The frequencies of the SIINFEKL-specific CD8<sup>+</sup> T cells in peripheral blood were high  $5.9 \pm 2.0\%$  ( $n = 5$ ) (compared to  $1.2 \pm 0.5\%$  at day 35 after the first boost and first tumor challenge). Antigen-specific T<sub>EM</sub> and T<sub>CM</sub> cell percentages were also rapidly increased after the recall, reaching the frequencies observed on day 35 after first immunization and boost, indicating mIONPsp-based vaccines induced T-cell memory and effective recall responses.

To evaluate the quality of CD8<sup>+</sup> T-cell responses, cellular extracts from spleen were cultured ex vivo and incubated with the antigenic peptide SIINFEKL for 5 h, and the IFN- $\gamma$  and TNF- $\alpha$  intracellular production, as well as the degranulation marker CD107a, were analyzed by flow cytometry. The data demonstrated that mice immunized with the nanoparticles generate T lymphocytes with enhanced cytolytic activity



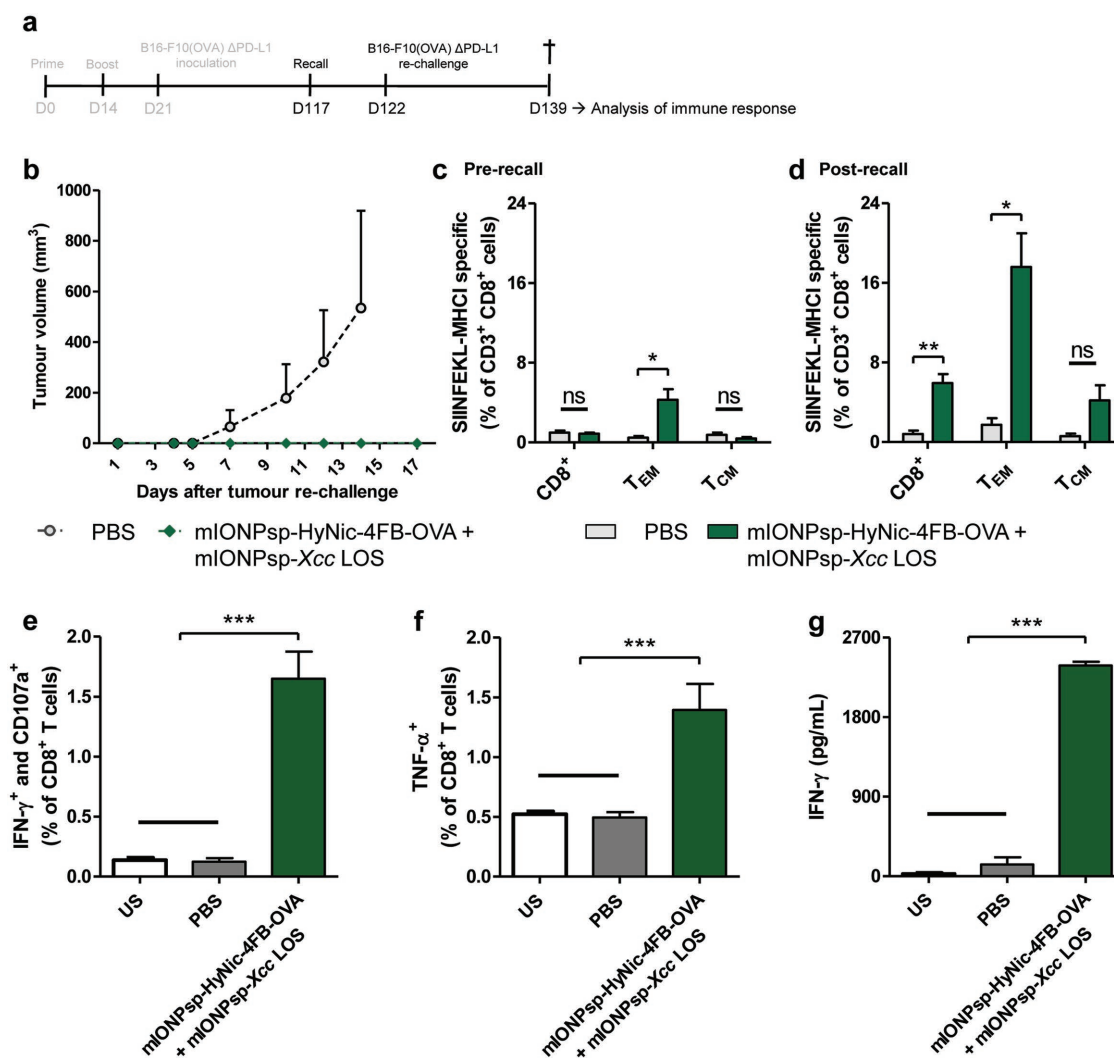


**Figure 8.** Tumor protection and rapid activation of the immune system upon recall of mIONPsp-based vaccines ( $n = 5$ ). a) 103 d after the first tumor inoculation, T-cell memory was recalled with the nanovaccines (same antigen/adjuvant concentrations). Five days after, a tumor rechallenge with  $2 \times 10^6$  B16-F10(OVA)  $\Delta$ PD-L1 cells was carried out. At day 17 after the second tumor challenge, mice were sacrificed and blood and spleens were collected for further immune analysis. b) Average tumor growth curves. c,d) SIINFEKL-specific CD8<sup>+</sup>, T<sub>EM</sub> and T<sub>CM</sub> cell percentages c) before and d) after recall injection. e,f) Intracellular IFN- $\gamma$  and TNF- $\alpha$  production and CD107a expression after 5 h of incubation with 10  $\mu$ g mL<sup>-1</sup> of SIINFEKL peptide. g) Extracellular IFN- $\gamma$  production after 48 h of incubation with the peptide. \*\*\* $P < 0.001$ , \*\* $P < 0.01$ , \* $P < 0.05$ , ns, nonsignificant by c,d) two-way ANOVA followed by Bonferroni's test and e–g) one-way ANOVA followed by Tukey's test.

(Figure 8e,f). Also, the cells collected from the spleen showed significantly enhanced ability to release IFN- $\gamma$  following ex vivo restimulation with SIINFEKL (over 48 h). Taken together, the results show the development of a potent and long lasting anti-tumor immunity when combining mIONPsp-based vaccines with PD-L1 abrogation.

### 3. Conclusion

In summary, we have designed and developed a cancer vaccine platform based on pathogen-mimicking TLR4 agonist functionalized nanostructures, which is significantly enhanced blocking the PD-1/L1 checkpoint. The system is composed of iron oxide NPs encapsulated in phospholipid micelles where the covalent

ligation of antigen was achieved by aniline-catalyzed hydrazone ligation, and the LOS derived from the plant pathogen *Xcc* as TLR4 agonist was adhered by hydrophobic interactions. We provided the first evidence that *Xcc* LOS elicits as adjuvant as potent immune responses as MPLA (FDA-approved TLR4 agonist) for the development of anticancer vaccines. However, this study also showed that unlike MPLA, the structurally unique *Xcc* LOS allows effective interaction with certain NP-filled micelles for the generation of stable pathogen-mimicking nanostructures with size, charge, and hydrophobicity ideal for lymph node delivery. The nanostructures with the best properties (size, stability, toxicity profile, and immune response) encapsulated the type of iron oxide NPs for which previous studies have shown effective in vivo tracking by multimodal imaging,<sup>[21,66]</sup> and ability to potentiate other cancer immunotherapies approaches

such as DC-based vaccination<sup>[32]</sup> and macrophage polarization into proinflammatory M1 phenotypes.<sup>[33]</sup> We showed that aniline-catalyzed hydrazone ligation enables highly efficient, monitorable, and stable covalent conjugation of tumor antigen for creating the multifunctional nanovaccines under physiological conditions at micromolar concentrations. The designed nanovaccines led to enhanced protection against highly aggressive and poorly immunogenic B16-F10 murine melanomas, and by abrogation of PD-L1 expression in the melanoma cells, they achieved complete tumor rejection in 100% of the immunized mice. Taken together, the study reveals the potential of *Xcc* LOS for development of anticancer vaccines and shows the general utility of creating nanovaccines based on pathogen-mimicking nanostructures and the hydrazone ligation reaction for antigen binding, as well as the importance of PD-L1 blockade for the significant “upgrading” vaccines exploiting TLR4 agonists.

#### 4. Experimental Section

**Bacterial Growth and LOS Extraction:** The lipooligosaccharide from *Xcc* was extracted and purified from dried cells as described in the Supporting Information and reported previously.<sup>[55,67]</sup>

**Synthesis and Characterization of Pathogen-Mimicking Micelles Encapsulating Iron Oxide Nanoparticles/Quantum Dots:** Hydrophobic spherical IONP (IONPsp) and cubic IONP (IONPc) were prepared according to published procedures.<sup>[68,69]</sup> To prepare control micelles and micelles for antigen conjugation, 1 mg of IONPsp, IONPc, or QDs and 2 mg of PEG phospholipids (phospholipid–PEG–OMe when preparing the micelles incorporating LPS/LOS and phospholipid–PEG–NH<sub>2</sub> for the conjugation of antigen) were dissolved in 100  $\mu$ L and 200  $\mu$ L of chloroform respectively, combined in a 4 mL round-bottomed flask with 100  $\mu$ L of chloroform and allowed to evaporate overnight at RT. The LOS- and LPS-coated micelles were prepared as described above with 0.2 mg of LOS or LPS dissolved in 100  $\mu$ L of chloroform. For fluorescent labeling of the micelles 5% of 1,2-dimyristoyl-*sn*-glycero-3-phosphoethanolamine-N-lissamine rhodamine B sulfonyl-ammonium salt was added to the phospholipid solution. The flask was placed in a water bath at 80 °C for 30 s, after which the resulting lipid film containing the nanoparticles was hydrated by adding 1 mL of MilliQ water. This solution was centrifuged (5000  $\times$  g, 5 min for mIONPsp and mQDs; 300  $\times$  g, 5 min for mIONPc) and passed through a 0.45  $\mu$ m sterile syringe filter to remove any nonsoluble or large particles. Then, the micelles were centrifuged (108 600  $\times$  g, 50 min for mIONPsp, 88 200  $\times$  g, 25 min for mIONPc; 108 600  $\times$  g, 45 min for mQDs); the supernatant was discarded (or analyzed for LPS/LOS content) and washed with MilliQ water to remove empty micelles and free ligands (three cycles). Finally, the pellet was dissolved in 400  $\mu$ L of MilliQ water (or 10  $\times$  10<sup>-3</sup> M phosphate buffered saline, PBS) and the nanoparticle-filled micelles were stored at 4 °C. Quantification of the iron concentration in the micelles was carried out by inductively coupled plasma atomic emission spectroscopy (ICP-AES) analysis. ICP-AES analyses were carried out on a Perkin Elmer Optima 5300 DV (Perkin Elmer, Santa Clara, CA, USA). The concentration of the QDs was determined from the optical absorption spectra according to Yu et al.<sup>[70]</sup> For this purpose, the absorption spectra of the mQDs solutions in the 200–800 nm range were recorded on a V-630Bio Spectrophotometer (JASCO Analytical Instruments).

Transmission electron microscopy (TEM) studies were performed using a JEOL JEM-2011 electron microscope operating at 120 kV. The samples were prepared by depositing a drop of a solution of the hydrophobic nanoparticles (1 mg mL<sup>-1</sup> in THF) onto Pelco 150 mesh grid (Ted Pella) and allowing it to dry. For the characterization of the hydrophilic samples, TEM grids were polarized using a Quorum technologies K100X glow discharge system. Nanoparticle size was determined from the TEM images measuring a minimum of 200

nanoparticles with the ImageJ software. Hydrodynamic diameter and  $\zeta$ -potential of the micelles were measured using a Z-Sizer (Malvern Nano-Zs, UK). To determine the stability, mIONPsp-*Xcc* LOS and mIONPsp-HyNic-4FB-OVA were dissolved in 10  $\times$  10<sup>-3</sup> M PBS and the hydrodynamic diameter analyzed by Z-Sizer immediately after purification and over a 4 week period. To measure the  $\zeta$ -potential, the samples were dissolved in 10  $\times$  10<sup>-3</sup> M NaCl and analyzed by Z-sizer.

**Conjugation of OVA Antigen to mIONPsp:** First, mIONPsp micelles were conjugated to HyNic (6-hydrazinonicotinamide acetone hydrazone) by coupling the succinimidyl ester (S-HyNic) to the amino groups of DSPE–PEG–amine. mIONPsp micelles (0.5–3  $\times$  10<sup>-6</sup> M) in 50  $\times$  10<sup>-3</sup> M NaPi buffer (pH 7.4) were reacted with a 1  $\times$  10<sup>-3</sup> M HyNic solution in CH<sub>3</sub>CN (NP:HyNic molar ratio  $\approx$ 2000:1). The reaction mixture was stirred overnight ( $\approx$ 14 h) at room temperature and the product was purified using a desalting column and a 0.5 mL centrifugal filter (100 kDa MW cutoff). Ovalbumin was modified with FB (succinimidyl 4-formylbenzoate). For this purpose, a 450  $\times$  10<sup>-6</sup> M endotoxin-free OVA solution in 50  $\times$  10<sup>-3</sup> M NaPi buffer (pH 7.4) was added to a 1  $\times$  10<sup>-3</sup> M FB solution in dimethyl sulfoxide (DMSO) (550  $\mu$ L total volume) and stirred overnight at room temperature. Purification was carried out using a desalting column and a 4 mL centrifugal filter (10 kDa MW cutoff). The product was stored at 4 °C until further use. Finally, the HyNic-modified mIONPsp ( $\approx$ 0.5–3  $\times$  10<sup>-6</sup> M) in 50  $\times$  10<sup>-3</sup> M NaPi buffer (pH 6.2) were reacted with the FB-modified OVA (20–30  $\times$  10<sup>-6</sup> M) in the presence of 100  $\times$  10<sup>-3</sup> M aniline. The reaction mixture was stirred overnight at room temperature and the product was purified by a desalting column and a 0.5 mL centrifugal filter (100 kDa MW cutoff). The obtained product was centrifuged at 17 400  $\times$  g for 20 min and the pellet washed with MilliQ water to remove unbound OVA.

**Quantification of LOS/LPS Loading:** The amount of LOS/LPS incorporated into the micelles was determined using a dose response curve obtained by measuring the amount of IL-6 released by J774A.1 macrophages stimulated overnight with the free ligands as a function of concentration. The amount of unbound LOS molecules present in each of the supernatants from each of the centrifugation cycles used for the purification of the NP-filled micelles was extrapolated from his calibration curve by measuring the amount of IL-6 released when the macrophages were incubated with the supernatants. For this purpose, a dose response calibration curve was obtained with *Xcc* LOS concentrations ranging from 3 to 36  $\times$  10<sup>-6</sup> M. IL-6 was measured in cell supernatants using sandwich ELISA following the manufacturer's instructions (vide infra). The amount of LPS was also determined using the FDA-approved limulus amoebocyte lysate (LAL) test. For this purpose, the analysis of LPS in the supernatants was performed using a Pierce LAL chromogenic endotoxin quantitation kit (ThermoFisher) following the instructions given by the manufacturer. The assay was performed in aseptic conditions. Briefly, 50  $\mu$ L of test sample were added to the test well in the 96-well plate at 37 °C and, incubated for 5 min after which the LAL reagent was added to each well. Following 10 min incubation, 100  $\mu$ L of substrate solution was added, stirred and incubated for 6 min. Then, 25  $\mu$ L of stop reagent solution was added and the absorbance at 405 nm was immediately measured using a Varioskan LUX multimode plate reader (Thermo Fisher). The concentration of LPS in the unknown samples was determined using a calibration curve.

***Xcc* LOS Release Studies:** *Xcc* LOS content in the micelles was measured immediately after purification and after 1 or 2 weeks. mIONPsp-*Xcc* LOS nanoparticles were centrifuged (108 600  $\times$  g, 50 min) and the supernatant was analyzed for *Xcc* LOS as described above.

**Cell Viability and Cytokine Production Experiments:** The J774A.1 mouse macrophage cell line was obtained from the American Type Culture Collection (ATCC) and was grown at 37 °C in a humidified atmosphere of 5% CO<sub>2</sub> using DMEM supplemented with 10% FBS and 1% P/S. Cell viability was determined using a 3-[4,5-dimethylthiazol-2-yl]-2,5 diphenyl tetrazolium bromide (MTT) assay. Briefly, cells were administered with 100  $\mu$ L per well of an MTT solution diluted in medium and incubated for 1 h at 37 °C, after which supernatants were discarded and MTT crystals dissolved in 200  $\mu$ L per well of DMSO. The absorbance of the wells was

measured using a TECAN Genios Pro 96/384 multifunction microplate reader at 550 nm and data represented as the cell viability compared to control wells. For obtaining the BMDC primary culture, C57BL/6j mice (6–12 weeks old) were sacrificed by cervical dislocation and intact femurs and tibiae of hind limbs were removed aseptically as described in the Supporting Information and reported elsewhere.<sup>[71]</sup>

**Quantification of Cytokine and Antibody Production by ELISA:** Cytokines were measured in cells' supernatants using IL-6, IL-12, or TNF- $\alpha$  sandwich ELISA. A four-parameter logistic standard curve was generated using Graph Pad prism 5 and used to get the cytokines concentrations. Results are expressed as mean  $\pm$  SEM in pg mL<sup>-1</sup> or ng mL<sup>-1</sup>. Anti-OVA IgG antibodies were measured in blood serum using indirect ELISA. The results were expressed as the log10 value of the reciprocal of the endpoint dilution that gave an optical density (O.D.) higher than the chosen cutoff, after the subtraction of background levels.

**Analysis of DCs' Maturation Markers by Flow Cytometry:** After overnight incubation with the different stimuli, 96-well plates containing the BMDCs were centrifuged (700  $\times$  g, 5 min, 4 °C) and supernatants were removed. Cells were stained with Alexa Fluor 488-labeled anti-CD11c, Brilliant Violet-labeled anti-CD80, PE-labeled anti-CD86, and APC-labeled anti-PD-L1 antibodies. Finally, cells were transferred to cytometry tubes by smooth pipetting. The expression of the different markers was analyzed using a FACS Canto II flow cytometer. BMDCs were electronically gated based on the forward and side scatter parameters and the not-single events left out based on forward area and height scatter parameters. DCs were gated based on positive staining for CD11c population marker and the expression of the chosen maturation markers was analyzed within this population (Figure S11a, Supporting Information). Results were expressed as mean  $\pm$  SEM of the MFI of each maturation marker of three independent experiments.

**Fluorescence Microscopy:** J774A.1 cells were seeded in an Ibidi  $\mu$ -Slide V1<sup>0.4</sup> at a density of 30 000 cells per well in supplemented DMEM and let to adhere overnight in an incubator maintained at 37 °C and 5% CO<sub>2</sub>. The day after, the medium was removed and cells were administered with 1  $\mu$ g mL<sup>-1</sup> Hoechst blue to stain the nuclei and incubated for 30 min. Cells were washed with PBS three times to remove unbound dye and then incubated with  $\approx 200 \times 10^{-9}$  M mIONPsp(Rho)-HyNic-4FB-OVA or mIONPsp(Rho)-Xcc LOS for 3 h. Cells were washed again and stained with 1  $\times 10^{-3}$  M LysoTracker green, incubated for 30 min, washed with PBS and finally images were taken using a ZEISS Axio Observer inverted microscope.

**In Vivo Studies:** Animals were cared for and handled in compliance with the Guidelines for Accommodation and Care of Animals (European Convention for the Protection of Vertebrate Animals Used for Experimental and Other Scientific Purposes) and internal guidelines, and all the experimental procedures were approved by the appropriate local authorities. All animals were housed in ventilated cages and fed on a standard diet ad libitum.

**Assessment of Antitumor Effect:** C57BL/6 mice (6–8 weeks old) were immunized subcutaneously in the flanks twice with an interval of 2 weeks between injections (100  $\mu$ L, 50  $\mu$ L per flank, 1  $\mu$ g of TLR4 ligands, 5  $\mu$ g of OVA and  $\approx 25$ –70  $\mu$ g of IONP per mice). On day 21 after first immunization, 3.5  $\times 10^5$  B16-F10(OVA) cells or 2  $\times 10^6$  B16-F10(OVA)  $\Delta$ PD-L1 cells diluted in PBS:Matrigel (1:1) were injected in the right back. Animals were monitored for tumor growth using an electronic digital caliper 779A series (Starrett). Criteria for humane endpoint included tumors greater than 1.5 cm diameter and ulceration. Results were expressed as mean  $\pm$  SEM of at least five mice per group. Blood was taken (50  $\mu$ L) at several time points after the first immunization for analyzing the generated immune response. In the case of antibodies production, blood was diluted in PBS and centrifuged (13 000  $\times$  g, 5 min) to separate the serum (supernatant) from blood cells (pellet). Blood sera were stored at -20 °C until its analysis by ELISA. In order to analyze the circulating cellular response, blood was diluted up to 4 mL in cold PBS. After centrifugation (1028  $\times$  g, 5 min at 4 °C), the pellet was resuspended in 2 mL of commercial RBC lysing buffer and incubated at RT. After washing the cell suspensions twice

with 5% FBS in PBS via centrifugation, cells were resuspended in complete RPMI-1640, ready for further analysis. Secondary lymphoid organs such as spleens were also harvested for the analysis of local cellular response. Briefly, spleens were harvested and perfused with tissue dissociating mix (3 mL of collagenase/DNase I diluted in RPMI-1640 medium), cut into small pieces and incubated for 30 min at RT in a sterile Petri dish. The reaction was stopped with 36  $\mu$ L of 500  $\times 10^{-3}$  M EDTA and organs were dissociated with the plunger of a syringe. RBC lysis was performed as previously described and the resulting cell suspensions were resuspended in complete RPMI-1640. Primary immune cells were analyzed for CD8<sup>+</sup> T cells, T<sub>CM</sub> and T<sub>EM</sub> cells specific for the OVA epitope SIINFEKL; extracellular and intracellular TNF- $\alpha$  and IFN- $\gamma$  production and CD107a degranulation marker expression were also analyzed. The quantification of extracellular IFN- $\gamma$  production was performed by seeding 8  $\times 10^5$  splenocytes per well, followed by incubation over 48 h with 10  $\mu$ g mL<sup>-1</sup> of SIINFEKL peptide and analyzing the supernatants by sandwich ELISA, as described above. For flow cytometry assays, 1  $\times 10^6$  splenocytes or peripheral blood cells were placed in round-bottom 96-well plates and stained with different antibodies. SIINFEKL-specific T cells were stained with Brilliant Violet 421-labeled anti-CD3, PE.Cy7-labeled anti-CD8, APC-labeled anti-CD44, FITC-labeled anti-CD62L and PE-labeled H-2kb-OVA<sub>257–264</sub> dextramer (Immudex). SIINFEKL specific cell percentage was analyzed in the CD8<sup>+</sup> T cell population (CD3<sup>+</sup> and CD8<sup>+</sup> double positive); in the T<sub>CM</sub> cell population (cells showing a phenotype of CD44<sup>low</sup> and CD62L<sup>low</sup> within CD3<sup>+</sup> and CD8<sup>+</sup> double positive population); and in the T<sub>EM</sub> population (CD44<sup>high</sup> and CD62L<sup>low</sup>) (Figure S11b, Supporting Information). To study intracellular TNF- $\alpha$  and IFN- $\gamma$  and the expression of the degranulation marker CD107a, cells were placed in 100  $\mu$ L of RPMI-1640 medium in the presence of Golgi Stop (BD Biosciences), PE-labeled anti-CD107a and 10  $\mu$ g mL<sup>-1</sup> SIINFEKL peptide. After 5 h of incubation at 37 °C, cells were washed twice and stained with the surface markers Brilliant Violet 421-labeled anti-CD3, Brilliant Violet 510-labeled anti-CD4 and FITC-labeled anti-CD8. Then, cells were fixed and permeabilized (cytofix/cytoperm fixation and permeabilization kit, BD Biosciences), after which intracellular cytokine staining was performed (APC-labeled anti-IFN- $\gamma$  and PE.Cy7-labelled anti-TNF- $\alpha$ ). T cells were gated based on double positive for CD3 and CD8 markers, excluding CD4<sup>+</sup> cells if needed. Results were represented as IFN- $\gamma$  and CD107a double positive or TNF- $\alpha$  positive cell percentage of total CD3<sup>+</sup> CD8<sup>+</sup> T cells. Isotype controls were added when needed but were not included in the figures for clarity purposes. Results were expressed as mean  $\pm$  SEM of five mice per group of immunization, analyzed individually, and compared to unstimulated wells.

**Statistical Analysis:** All data presented were expressed as mean  $\pm$  SEM. The differences between the control and the experimental groups were assessed using one- or two-way ANOVA followed by Tukey's test or Bonferroni's test (GraphPad Prism, GraphPad Software, La Jolla, CA). *P* values of less than 0.05 were considered statistically significant.

## Supporting Information

Supporting Information is available from the Wiley Online Library or from the author.

## Acknowledgements

This work was supported by H2020-MSCA-ITN-2014-ETN TOLLerant (grant agreement 642157), M-ERA.NET-2015 MediSURF (Reference Number: project 3193), and by the Spanish Ministry of Economy and Competitiveness Grant CTQ2014-54761-R and PCIN-2016-085. The authors are grateful to Dr. Pablo Sarobe (Centre for Applied Medical Research, CIMA, Universidad de Navarra, Pamplona, Spain) for providing the B16-F10(OVA) cells.

## Conflict of Interest

The authors declare no conflict of interest.

## Keywords

checkpoint inhibition, drug delivery, immunotherapy, magnetic nanoparticles, Toll-like receptor 4 agonists, vaccines

Received: September 27, 2018

Revised: November 7, 2018

Published online:

- [1] M. A. Postow, M. K. Callahan, J. D. Wolchok, *J. Clin. Oncol.* **2015**, *33*, 1974.
- [2] B. D. Shields, F. Mahmoud, E. M. Taylor, S. D. Byrum, D. Sengupta, B. Koss, G. Baldini, S. Ransom, K. Cline, S. G. Mackintosh, R. D. Edmondson, S. Shalin, A. J. Tackett, *Sci. Rep.* **2017**, *7*, 807.
- [3] C. F. Friedman, T. A. Proverbs-Singh, M. A. Postow, *JAMA Oncol.* **2016**, *2*, 1346.
- [4] S. Kato, A. Goodman, V. Walavalkar, D. A. Barkauskas, A. Sharabi, R. Kurzrock, *Clin. Cancer Res.* **2017**, *23*, 4242.
- [5] S. Champiat, L. Derclé, S. Ammari, C. Massard, A. Hollebecque, S. Postel-Vinay, N. Chaput, A. Eggermont, A. Marabelle, J.-C. Soria, C. Féré, *Clin. Cancer Res.* **2017**, *23*, 1920.
- [6] R. W. Jenkins, D. A. Barbie, K. T. Flaherty, *Br. J. Cancer* **2018**, *118*, 9.
- [7] B. Mastelic, S. Ahmed, W. M. Egan, G. Del Giudice, H. Golding, I. Gust, P. Neels, S. G. Reed, R. L. Sheets, C.-A. Siegrist, P. H. Lambert, *Biologicals* **2010**, *38*, 594.
- [8] S. Akira, K. Takeda, T. Kaisho, *Nat. Immunol.* **2001**, *2*, 675.
- [9] C. Maisonneuve, S. Bertholet, D. J. Philpott, E. De Gregorio, *Proc. Natl. Acad. Sci. USA* **2014**, *111*, 12294.
- [10] J. K. Dowling, A. Mansell, *Clin. Transl. Immunol.* **2016**, *5*, e85.
- [11] C. N. Baxevanis, I. F. Voutsas, O. E. Tsitsilonis, *Immunotherapy* **2013**, *5*, 497.
- [12] S. Kaczanowska, A. M. Joseph, E. Davila, *J. Leukocyte Biol.* **2013**, *93*, 847.
- [13] H. Lu, *Front. Immunol.* **2014**, *5*, 83.
- [14] S. Karaki, M. Anson, T. Tran, D. Giusti, C. Blanc, S. Oudard, E. Tartour, *Vaccines* **2016**, *4*, 37.
- [15] S. T. Reddy, A. J. van der Vlies, E. Simeoni, V. Angeli, G. J. Randolph, C. P. O'Neil, L. K. Lee, M. A. Swartz, J. A. Hubbell, *Nat. Biotechnol.* **2007**, *25*, 1159.
- [16] J. J. Moon, H. Suh, A. Bershteyn, M. T. Stephan, H. Liu, B. Huang, M. Sohail, S. Luo, S. H. Um, H. Khant, J. T. Goodwin, J. Ramos, W. Chiu, D. J. Irvine, *Nat. Mater.* **2011**, *10*, 243.
- [17] S. Yan, B. E. Rolfe, B. Zhang, Y. H. Mohammed, W. Gu, Z. P. Xu, *Biomaterials* **2014**, *35*, 9508.
- [18] A. de Titta, M. Ballester, Z. Julier, C. Nembrini, L. Jeanbart, A. J. van der Vlies, M. A. Swartz, J. A. Hubbell, *Proc. Natl. Acad. Sci. USA* **2013**, *110*, 19902.
- [19] J. T. Wilson, S. Keller, M. J. Manganiello, C. Cheng, C.-C. Lee, C. Opara, A. Convertine, P. S. Stayton, *ACS Nano* **2013**, *7*, 3912.
- [20] I. H. Lee, H. K. Kwon, S. An, D. Kim, S. Kim, M. K. Yu, J. H. Lee, T. S. Lee, S. H. Im, S. Jon, *Angew. Chem., Int. Ed.* **2012**, *51*, 8800.
- [21] A. Ruiz-de-Angulo, A. Zabaleta, V. Gómez-Vallejo, J. Llop, J. C. Mareque-Rivas, *ACS Nano* **2016**, *10*, 1602.
- [22] H. Liu, K. D. Moynihan, Y. Zheng, G. L. Szeto, A. V. Li, B. Huang, D. S. Van Egeren, C. Park, D. J. Irvine, *Nature* **2014**, *507*, 519.
- [23] C.-C. Chang, M. Campoli, S. Ferrone, *Curr. Opin. Immunol.* **2004**, *16*, 644.
- [24] H. Li, Y. Li, J. Jiao, H.-M. Hu, *Nat. Nanotechnol.* **2011**, *6*, 645.
- [25] J. Xiang, L. Xu, H. Gong, W. Zhu, C. Wang, J. Xu, L. Feng, L. Cheng, R. Peng, Z. Liu, *ACS Nano* **2015**, *9*, 6401.
- [26] J. P. M. Almeida, A. Y. Lin, E. R. Figueroa, A. E. Foster, R. A. Drezek, *Small* **2015**, *11*, 1453.
- [27] Z. R. Stephen, F. M. Kievit, M. Zhang, *Mater. Today* **2011**, *14*, 330.
- [28] C. Rümennapp, B. Gleich, A. Haase, *Pharm. Res.* **2012**, *29*, 1165.
- [29] A. C. Anselmo, S. Mitragotri, *AAPS J.* **2015**, *17*, 1041.
- [30] R. A. Revia, M. Zhang, *Mater. Today* **2016**, *19*, 157.
- [31] J. E. Rosen, L. Chan, D. Bin Shieh, F. X. Gu, *Nanomed.: Nanotechnol. Biol. Med.* **2012**, *8*, 275.
- [32] N.-H. Cho, T.-C. Cheong, J. H. Min, J. H. Wu, S. J. Lee, D. Kim, J.-S. Yang, S. Kim, Y. K. Kim, S.-Y. Seong, *Nat. Nanotechnol.* **2011**, *6*, 675.
- [33] S. Zanganeh, G. Hutter, R. Spitler, O. Lenkov, M. Mahmoudi, A. Shaw, J. S. Pajarinen, H. Nejadnik, S. Goodman, M. Moseley, L. M. Coussens, H. E. Daldrop-Link, *Nat. Nanotechnol.* **2016**, *11*, 986.
- [34] W. R. Algar, D. E. Prasuhan, M. H. Stewart, T. L. Jennings, J. B. Blanco-Canosa, P. E. Dawson, I. L. Medintz, *Bioconjugate Chem.* **2011**, *22*, 825.
- [35] J. B. Blanco-Canosa, I. L. Medintz, D. Farrell, H. Mattoussi, P. E. Dawson, *J. Am. Chem. Soc.* **2010**, *132*, 10027.
- [36] C. W. Cluff, in *Lipid A in Cancer Therapy* (Ed: J.-F. Jeannin), Springer, New York, NY **2009**, pp. 111–123.
- [37] S. L. Giannini, E. Hanon, P. Moris, M. Van Mechelen, S. Morel, F. Dessy, M. A. Fourneau, B. Colau, J. Suzich, G. Losonksy, M. T. Martin, G. Dubin, M. A. Wettendorff, *Vaccine* **2006**, *24*, 5937.
- [38] A. M. Didierlaurent, S. Morel, L. Lockman, S. L. Giannini, M. Bisteau, H. Carlsen, A. Kielland, O. Vosters, N. Vanderheyde, F. Schiavetti, D. Larocque, M. Van Mechelen, N. Garçon, *J. Immunol.* **2009**, *183*, 6186.
- [39] M. K. L. MacLeod, A. S. McKee, A. David, J. Wang, R. Mason, J. W. Kappler, P. Marrack, *Proc. Natl. Acad. Sci. USA* **2011**, *108*, 7914.
- [40] C. M. Paulos, A. Kaiser, C. Wrzesinski, C. S. Hinrichs, L. Cassard, A. Boni, P. Muranski, L. Sanchez-Perez, D. C. Palmer, Z. Yu, P. A. Antony, L. Gattinoni, S. A. Rosenberg, N. P. Restifo, *Clin. Cancer Res.* **2007**, *13*, 5280.
- [41] Y. J. Cho, B. Y. Ahn, N. G. Lee, D. H. Lee, D.-S. Kim, *Vaccine* **2006**, *24*, 5862.
- [42] D. M. Pardoll, *Nat. Rev. Cancer* **2012**, *12*, 252.
- [43] V. Pulko, X. Liu, C. J. Krco, K. J. Harris, X. Frigola, E. D. Kwon, H. Dong, *J. Immunol.* **2009**, *183*, 3634.
- [44] A. Varthaman, H. D. Moreau, M. Maurin, P. Benaroch, *PLoS One* **2016**, *11*, e0167057.
- [45] T. Fukaya, H. Takagi, Y. Sato, K. Sato, K. Eizumi, H. Taya, T. Shin, L. Chen, C. Dong, M. Azuma, H. Yagita, B. Malissen, K. Sato, *Blood* **2010**, *116*, 2266.
- [46] L. M. Francisco, V. H. Salinas, K. E. Brown, V. K. Vanguri, G. J. Freeman, V. K. Kuchroo, A. H. Sharpe, *J. Exp. Med.* **2009**, *206*, 3015.
- [47] J. Lau, J. Cheung, A. Navarro, S. Lianoglou, B. Haley, K. Totpal, L. Sanders, H. Koepfen, P. Caplazi, J. McBride, H. Chiu, R. Hong, J. Grogan, V. Javinal, R. Yauch, B. Irving, M. Belvin, I. Mellman, J. M. Kim, M. Schmidt, *Nat. Commun.* **2017**, *8*, 14572.
- [48] M. Gato-Cañás, M. Zuazo, H. Arasanz, M. Ibañez-Vea, L. Lorenzo, G. Fernandez-Hinojal, R. Vera, C. Smerdou, E. Martisova, I. Arozarena, C. Wellbrock, D. Llopiz, M. Ruiz, P. Sarobe, K. Breckpot, G. Kochan, D. Escors, *Cell Rep.* **2017**, *20*, 1818.
- [49] A. I. Bocanegra Gondan, A. Ruiz-de-Angulo, A. Zabaleta, N. Gómez Blanco, B. M. Cobaleda-Siles, M. J. García-Granda, D. Padro, J. Llop, B. Arnaiz, M. Gato, D. Escors, J. C. Mareque-Rivas, *Biomaterials* **2018**, *170*, 95.
- [50] H. Liu, D. J. Irvine, *Bioconjugate Chem.* **2015**, *26*, 791.
- [51] D. A. Rao, M. L. Forrest, A. W. G. Alani, G. S. Kwon, J. R. Robinson, *J. Pharm. Sci.* **2010**, *99*, 2018.



- [52] F. Ahsan, I. P. Rivas, M. A. Khan, A. I. Torres Suárez, *J. Controlled Release* **2002**, *79*, 29.
- [53] Y. Tabata, Y. Ikada, *Biomaterials* **1988**, *9*, 356.
- [54] S. Smulders, J.-P. Kaiser, S. Zuin, K. L. Van Landuyt, L. Golanski, J. Vanoirbeek, P. Wick, P. H. Hoet, *Part. Fibre Toxicol.* **2012**, *9*, 41.
- [55] A. Silipo, A. Molinaro, L. Sturiale, J. M. Dow, G. Erbs, R. Lanzetta, M.-A. Newman, M. Parrilli, *J. Biol. Chem.* **2005**, *280*, 33660.
- [56] A. Silipo, A. Molinaro, R. Lanzetta, M. Parrilli, B. Lindner, O. Holst, *Eur. J. Org. Chem.* **2004**, *2004*, 1336.
- [57] A. Rice, J. Wereszczynski, *Biophys. J.* **2018**, *114*, 1389.
- [58] P. G. Adams, L. Lamoureux, K. L. Swingle, H. Mukundan, G. A. Montaño, *Biophys. J.* **2014**, *106*, 2395.
- [59] A. E. Gregory, E. D. Williamson, J. L. Prior, W. A. Butcher, I. J. Thompson, A. M. Shaw, R. W. Titball, *Vaccine* **2012**, *30*, 6777.
- [60] C. Nembrini, A. Stano, K. Y. Dane, M. Ballester, A. J. van der Vlies, B. J. Marsland, M. A. Swartz, J. A. Hubbell, *Proc. Natl. Acad. Sci. USA* **2011**, *108*, E989.
- [61] M. Mueller, B. Lindner, S. Kusumoto, K. Fukase, A. B. Schromm, U. Seydel, *J. Biol. Chem.* **2004**, *279*, 26307.
- [62] S. Akira, K. Takeda, *Nat. Rev. Immunol.* **2004**, *4*, 499.
- [63] H. Husebye, Ø. Halaas, H. Stenmark, G. Tunheim, Ø. Sandanger, B. Bogen, A. Brech, E. Latz, T. Espevik, *EMBO J.* **2006**, *25*, 683.
- [64] N. S. Butler, J. C. Nolz, J. T. Harty, *Cell. Microbiol.* **2011**, *13*, 925.
- [65] F. Sallusto, D. Lenig, R. Förster, M. Lipp, A. Lanzavecchia, *Nature* **1999**, *401*, 708.
- [66] M. Cobaleda-Siles, M. Henriksen-Lacey, A. R. de Angulo, A. Bernecker, V. G. Vallejo, B. Szczupak, J. Llop, G. Pastor, S. Plaza-Garcia, M. Jauregui-Osoro, L. K. Meszaros, J. C. Mareque-Rivas, *Small* **2014**, *10*, 5053.
- [67] F. Di Lorenzo, A. Palmigiano, A. Silipo, Y. Desaki, D. Garozzo, R. Lanzetta, N. Shibuya, A. Molinaro, *Carbohydr. Res.* **2016**, *427*, 38.
- [68] S. Shouheng, H. Zeng, D. B. Robinson, S. Raoux, P. M. Rice, S. X. Wang, G. Li, *J. Am. Chem. Soc.* **2004**, *126*, 273.
- [69] N. Lee, Y. Choi, Y. Lee, M. Park, W. K. Moon, S. H. Choi, T. Hyeon, *Nano Lett.* **2012**, *12*, 3127.
- [70] W. William Yu, L. Qu, W. Guo, X. Peng, *Chem. Mater.* **2003**, *15*, 2854.
- [71] M. B. Lutz, N. Kukutsch, A. L. Ogilvie, S. Rössner, F. Koch, N. Romani, G. Schuler, *J. Immunol. Methods* **1999**, *223*, 77.